Received 26 August 2017; | Revised 12 July 2018; | Accepted XX 2018

DOI: xxx/xxxx

ARTICLE TYPE

XFEM formulation with sub-interpolation, and equivalence to zero-thickness interface elements

Laura Crusat | Ignacio Carol | Daniel Garolera

[1]Department of Civil and Environmental Engineering, Division of Geotechnical Engineering, BarcelonaTech (UPC), Campus Nord, 08034 Barcelona, Spain

Correspondence
Laura Crusat Email: laura.crusat@upc.edu,
Ignacio Carol Email: ignacio.carol@upc.edu

Summary

This paper describes a particular formulation of the eXtended Finite Element Method (XFEM) specifically conceived for application to existing discontinuities of fixed location, for instance in geological media. The formulation is based on two non-standard assumptions: (1) the use of sub-interpolation functions for each subdomain, and (2) the use of fictitious displacement variables on the nodes across the discontinuity (instead of the more traditional jump variables). Thanks to the first of those assumptions, the proposed XFEM formulation may be shown to be equivalent to the standard Finite Element Method with zero-thickness interface elements for the discontinuities (FEM+z). The said equivalence is theoretically proven for the case of quadrangular elements cut in two quadrangles by the discontinuity, and only approximate for other types of intersections of quadrangular or triangular elements, in which the XFEM formulation corresponds to a kinematically restricted version of the corresponding interface plus continuum scheme. The proposed XFEM formulation with sub-interpolation, also helps improving spurious oscillations of the results obtained with natural interpolation functions when the discontinuity runs skew to the mesh. A possible explanation for these oscillations is provided, which also explains the improvement observed with sub-interpolation. The paper also discusses the oscillations observed in the numerical results when some nodes are too close to the discontinuity, and proposes the remedy of moving those nodes onto the discontinuity itself. All the aspects discussed are illustrated with some examples of application, the results of which are compared to closed-form analytical solutions or to existing XFEM results from the literature.

KEYWORDS:
Fracture mechanics; crack; XFEM; zero-thickness elements; fictitious displacement; reinterpolation

1 | INTRODUCTION

Discontinuities play an important role in many types of solid mechanics problems, and their role may be crucial in specific fields such as Geomechanics. The discontinuous displacement field associated to the presence of discontinuities has been incorporated in the FE analysis using different techniques such as standard continuum elements with appropriate softening

laws (traditional "smeared approach",[1–3]), interface elements ("discrete approach"[4–6]), elements with embedded discontinuities[7–10], or the extended finite element method (XFEM,[11–16]).

The Extended Finite Element Method (XFEM) is a relatively recent method used to model discontinuities which has evolved as a particular case of the Partition of Unity Method (PUM) or the Partition of Unity Finite Element Method (PUFEM). The main idea of this method is to enrich the standard basis that describe the continuum field of displacements, with some additional modes of deformation that describe the discontinuities in the field. The main difference with other options such as embedded discontinuities, is that the additional XFEM variables are nodal variables shared by adjacent elements, which means that the jump values at the discontinuity will be continuous across elements, therefore guaranteeing a conformity in the solution similar for instance to that obtained with zero-thickness interface elements (but not for instance with most formulations of the "embedded discontinuity" type, in which the jump variables are internal to each element, without any continuity enforced).

Most existing XFEM formulations for solid mechanics (e.g.[17–21]) use the relative ("jump") displacements as additional variables at the nodes of the elements crossed by the discontinuity. In this case, however, the fictitious "overhang" displacements across the discontinuity, as described in[22], have been preferred over the jumps themselves, because of a clearer physical meaning, which makes more intuitive to establish the formulation, and especially to impose the necessary boundary conditions.

Another common feature of most existing XFEM formulation is the use of natural interpolation functions (the functions of the original continuum element) to interpolate the displacement within the element subdomains. In this paper the new approach of sub-interpolation is proposed, by which the original element functions are used exclusively to interpolate the displacement values from the original element nodes to the points of intersection of the discontinuity with the element edges, while new sub-interpolation functions are used within each element sub-domain.

A reported issue of existing XFEM formulations is the oscillation observed in the results when discontinuity runs skew to the mesh[23,24], which is linked to the use of the natural interpolation scheme. According to this interpretation, the new scheme with sub-interpolation should helps avoiding this problem. This improvement seems confirmed by a basic example of application provided.

A theoretical aspect of the XFEM that seems not dealt with in the existing literature is the relation and possible equivalence to the traditional approach of standard FEM with zero-thickness interface elements along the same discontinuity location[4], since both approaches seem similar conceptually in that both describe the jump by using new field variables that are shared by adjacent elements. Also, in both approaches the constitutive behavior of the discontinuity may be described in terms of the same variables, namely relative (normal and shear) displacements, and stress tractions (also normal and shear), and therefore the same constitutive equations may be used. In this paper, this equivalence is explored successfully for the XFEM formulation proposed and a "2-2" quadrangular element configuration (the discontinuity line divides the element leaving two nodes on each side). The expression of the XFEM stiffness matrix is derived, and the equivalence is shown to the assembly of the stiffness matrices of the continuum and zero-thickness interface elements for the same configuration.

Another aspect of concern for the numerical application of XFEM formulations, is the spurious oscillations reported on the values of normal and shear stress on the discontinuity itself (e.g.[23–25]), when the discontinuity line runs too close to a mesh node. These oscillations may be critical to then check shear sliding conditions, and therefore evaluate failure loads and safety factors. This problem is also examined in the paper, by first identifying the appearance of such oscillations at locations where nodes are too close to the discontinuity location and the intersection with surrounding finite elements leads to very small or badly shaped element subdivisions. A common remedy for this problem is to move the nodes away from the discontinuity so that element sizes and aspect ratios improve[26]. However, the way to do this is not unique, and improvements are not drastic, which motivates to propose a new strategy consisting of the opposite: bringing the nodes onto the discontinuity itself. Although it requires identifying some additional element configurations, this strategy is developed in the paper and shown to be very efficient, eliminating oscillations without producing other distorted elements in the vicinity. The improvement obtained with this strategy is also justified on the basis of the count of independent kinematic variables of the element.

This article is organized as follows: After this introduction, Section 2 describes general XFEM concepts and the detailed XFEM formulation proposed, including the derivation of the stiffness matrices and force vectors based on the Principle of Virtual Work. Although conceptually not new, to the knowledge of the authors this type of derivation seems not available in existing XFEM literature. Section 3, discusses moving nodes to the discontinuity and resulting special configurations. In Section 4, the equivalence between the XFEM and zero-thickness interface elements is demonstrated for the "2-2" quadrangular configuration, and other configurations are discussed. Section 5 reports the numerical results obtained with the proposed formulation for three examples of application. These results are compared to either closed-form solution or to other numerical results from the

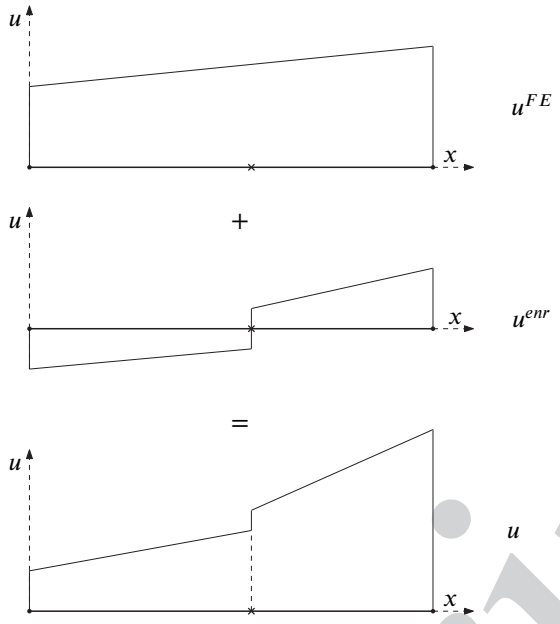

FIGURE 1 Graphical representation of the general equation of XFEM (1)

literature. Finally, Section 6 summarizes the main achievements of the paper and gives some concluding remarks. Appendices A to C include specific expressions of the formulation matrices for quadrangular and triangular elements. Appendix D includes a review of the standard natural interpolation scheme, with the possible explanation for the oscillations observed in the case of a skew discontinuity. An example of application showing comparison with new sub-interpolation scheme is also provided.

2 | XFEM FORMULATION

2.1 | General concepts and additional variables

The essential idea of the Extended Finite Element Method (XFEM) consists of enriching the standard finite element with extra degrees of freedom at the nodes, in order to represent a discontinuous field within the element. Considering $\boldsymbol{x}$ as any point within the element, and assuming the existence of a field discontinuity within the element domain, the displacement vector $\boldsymbol{u}$ at any point within the element is expressed as the sum of two contributions from the standard continuum field, $\boldsymbol{u}^{FE}$ and from the enrichment functions, $\boldsymbol{u}^{enr}$, according to the expression:

$$\boldsymbol{u}(\boldsymbol{x}) = \boldsymbol{u}^{FE} + \boldsymbol{u}^{enr} = \sum_{k=1}^{n} N_{(k)}(\boldsymbol{x})\boldsymbol{u}_{(k)} + \sum_{i=1}^{m} N_{(i)}(\boldsymbol{x})\,\psi_{(i)}(\boldsymbol{x})\boldsymbol{a}_{(i)} \tag{1}$$

where $N_{(k)}$ are the shape functions for the regular (continuum) part of the displacements represented by regular degrees of freedom at the nodes, $\boldsymbol{u}_{(k)}$ ($k = 1, 2 \ldots n$, number of nodes), while $\boldsymbol{a}_{(i)}$ are the additional nodal variables, and functions $\psi_{(i)}$ ($i = 1, 2 \ldots m$, number of enrichments which is generally equal to n) represent the corresponding enrichment functions.

Note that with the above expression, in the case that $\boldsymbol{a}_{(i)} = \boldsymbol{0}$, (i.e. all enrichment nodal values equal to zero), the second term disappears and the regular FE interpolation is recovered. On the other hand, in the general case that the enrichment nodal values $\boldsymbol{a}_{(i)}$ are non-zero, the two contributions above lead to a picture such as Fig 1 , in which the continuum and enriched parts sum up to obtain the total XFEM displacement field.

For the enrichment function $\psi_{(i)}(\boldsymbol{x})$ different forms have been proposed. Note that (as represented in Fig. 1) some choices of this function with non-zero values at the nodes may make the final value of displacements at the nodes ($\boldsymbol{u}$) different from the regular displacement variables at those nodes ($\boldsymbol{u}_{(k)}$). This inconvenient feature can be avoided by using the following definition based on the Heaviside function ([22]):

$$H(\boldsymbol{x}) = \begin{cases} 0 & \boldsymbol{x} \in \Omega^{-} \\ 1 & \boldsymbol{x} \in \Omega^{+} \end{cases} \tag{2}$$

TABLE 1 Enrichment function, $\psi_{(i)}(\boldsymbol{x})$.

Point ($\boldsymbol{x}$)	Domain ($\Omega^{\pm}_{(i)}$)	$H(\boldsymbol{x})$	-	$H(\Omega^{\pm}_{(i)})$	=	$\psi_{(i)}(\boldsymbol{x})$
$\boldsymbol{x} \in \Omega^{-}$	Ω^{-}	0	-	0	=	0
	Ω^{+}	0	-	1	=	-1
$\boldsymbol{x} \in \Omega^{+}$	Ω^{-}	1	-	0	=	1
	Ω^{+}	1	-	1	=	0

$$\psi_{(i)}(\boldsymbol{x}) = H(\boldsymbol{x}) - H\left(\Omega^{\pm}_{(i)}\right) \tag{3}$$

where $\Omega^{\pm}_{(i)}$ indicates the element subdomain (left or right of the discontinuity). Particularizing the enrichment function (3) for each sub-domain, the resulting values of $\psi_{(i)}(\boldsymbol{x})$ are obtained (shown in Table 1), and represented in Fig. 2 b. Combining the above function $\psi_{(i)}(\boldsymbol{x})$ with the standard linear shape functions, leads in the case of 1-D elements to the overall interpolation functions for the additional degrees of freedom $\boldsymbol{a}_{(i)}$ that are depicted in Fig. 2 c, in which, in order to simplify notation, the following variables are used within each subdomain:

$$\boldsymbol{x}^{-} \overset{def}{=} \boldsymbol{x} \in \Omega^{-}, \quad \boldsymbol{x}^{+} \overset{def}{=} \boldsymbol{x} \in \Omega^{+}, \quad \boldsymbol{x}^{J} \overset{def}{=} \boldsymbol{x} \in \Omega^{J} \tag{4}$$

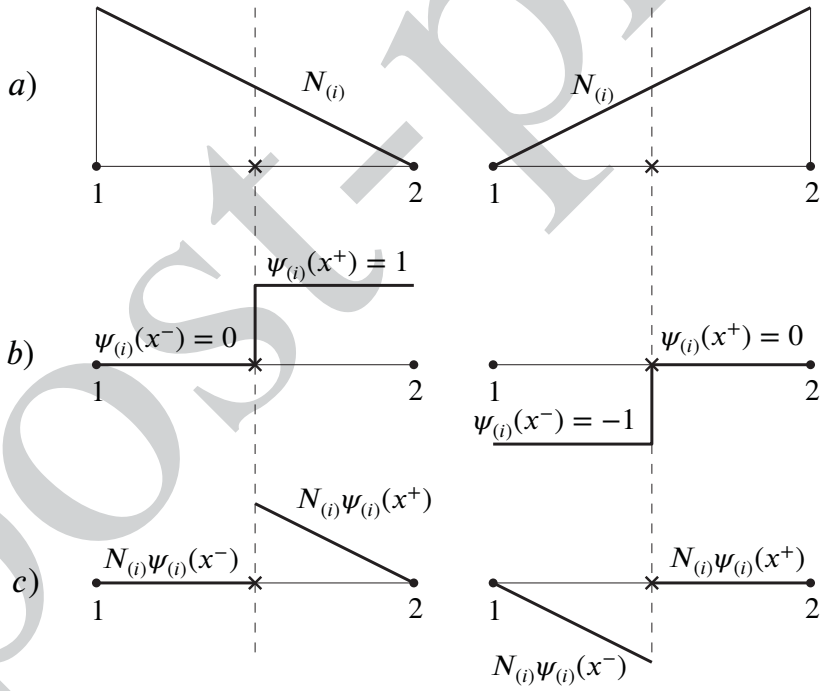

FIGURE 2 Graphical representation of (a) shape functions $\left(N_{(i)}\right)$ (b) enrichment function ($\psi_{(i)}$) and (c) product of them.

2.2 | Choice of fictitious "overhang" displacements as additional nodal variables

The interpolation in terms of the displacement jump $\boldsymbol{a}$ is the most common in XFEM literature. However, due to some advantages in the definition of the boundary conditions, in the present implementation it was decided to operate with some alternative nodal

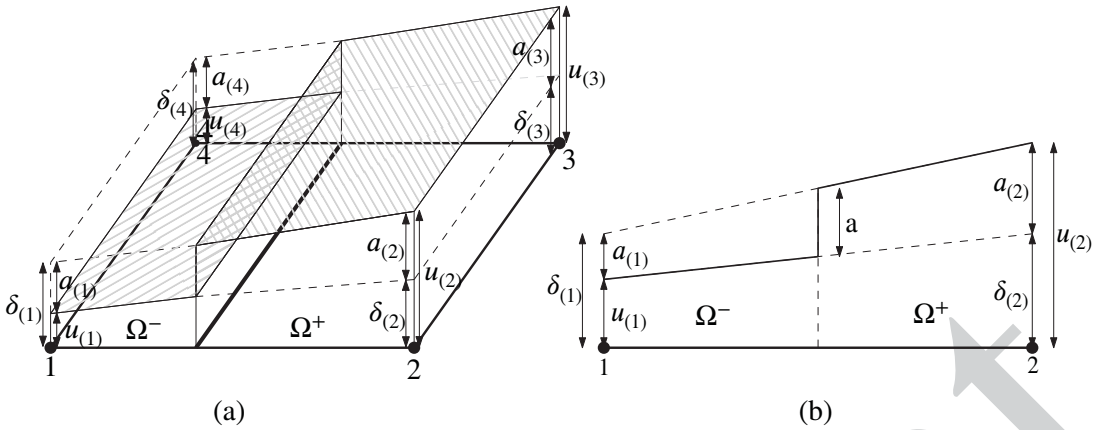

FIGURE 3 (a) Displacement field representation of a quadrangular element. Filled surfaces represent the real displacements and dashed lines the fictitious displacement. Also, subtracting real and fictitious displacements the jump is obtained. (b) One-dimensional representation of real displacement (u), fictitious displacement (δ) and jump (a).

variables to describe the discontinuity values: the fictitious displacements $\boldsymbol{\delta}$ of the "overhang" nodes across the discontinuity. This choice was proposed in[22], and is represented in Fig. 3 , together with regular nodal displacements $\boldsymbol{u}$ and the nodal jumps $\boldsymbol{a}$.

As shown in Figures 3 a and 3 b, the relation between $\boldsymbol{\delta}_{(i)}$, $\boldsymbol{u}_{(i)}$ and $\boldsymbol{a}_{(i)}$ is slightly different for the nodes on one side or the other of the discontinuity, as given by expressions:

$$\begin{cases} \boldsymbol{\delta}_{(i)} = \boldsymbol{u}_{(i)} + \boldsymbol{a}_{(i)} & in \ \ \Omega^- \\ \boldsymbol{\delta}_{(i)} = \boldsymbol{u}_{(i)} - \boldsymbol{a}_{(i)} & in \ \ \Omega^+ \end{cases} \tag{5}$$

From these equations one can isolate $\boldsymbol{a}_{(i)}$ and replace into Eq.(1), which leads to the expressions for the interpolation of displacements $\boldsymbol{u}(\boldsymbol{x})$ in terms of the regular nodal displacements $\boldsymbol{u}_{(i)}$ and the alternative XFEM nodal variables $\boldsymbol{\delta}_{(i)}$:

$$\boldsymbol{u}\left(\boldsymbol{x}^-\right) = \sum_{i\in\Omega^-} N_{(i)}\boldsymbol{u}_{(i)} + \sum_{i\in\Omega^+} N_{(i)}\boldsymbol{\delta}_{(i)} \tag{6}$$

$$\boldsymbol{u}\left(\boldsymbol{x}^+\right) = \sum_{i\in\Omega^-} N_{(i)}\boldsymbol{\delta}_{(i)} + \sum_{i\in\Omega^+} N_{(i)}\boldsymbol{u}_{(i)} \tag{7}$$

That is, the interpolation in terms of $\boldsymbol{\delta}_{(i)}$ is always based on the regular standard shape functions, although it involves selectively the regular displacements $\boldsymbol{u}_{(i)}$ for those nodes on the same side of the discontinuity as the point at which the function is being evaluated, and the fictitious "overhang" displacements $\boldsymbol{\delta}_{(i)}$ for the rest of the nodes on the opposite side. Graphical interpretation is intuitive from Fig. 3 , and the jump itself may be also expressed in a relatively simple way as:

$$\boldsymbol{a}\left(\boldsymbol{x}^J\right) = \boldsymbol{u}\left(\boldsymbol{x}^+\right) - \boldsymbol{u}\left(\boldsymbol{x}^-\right) \tag{8}$$

$$\boldsymbol{a}\left(\boldsymbol{x}^J\right) = \sum_{i\in\Omega^-} N_{(i)}\left(\boldsymbol{\delta}_{(i)} - \boldsymbol{u}_{(i)}\right) + \sum_{i\in\Omega^+} N_{(i)}\left(\boldsymbol{u}_{(i)} - \boldsymbol{\delta}_{(i)}\right) \tag{9}$$

2.3 | Natural Interpolation vs double interpolation ("sub-interpolation") functions

In XFEM literature, interpolation over the element subdomains is usually made using the standard shape functions of the original element (Fig. 4 a). However, as discussed in Appendix D which includes an example of application, this interpolation leads to a reasonable representation only if the discontinuity is parallel to faces of the element. Overcoming these difficulties for the general case of discontinuities running skew to the mesh, is the motivations of the "double interpolation" (or sub-interpolation) scheme described in the following.

Consider the four-node linear rectangular element shown in Fig. 4 a, crossed by a discontinuity in configuration "2-2" as shown in Fig.5 . The double interpolation scheme considered in this study, involves two steps:

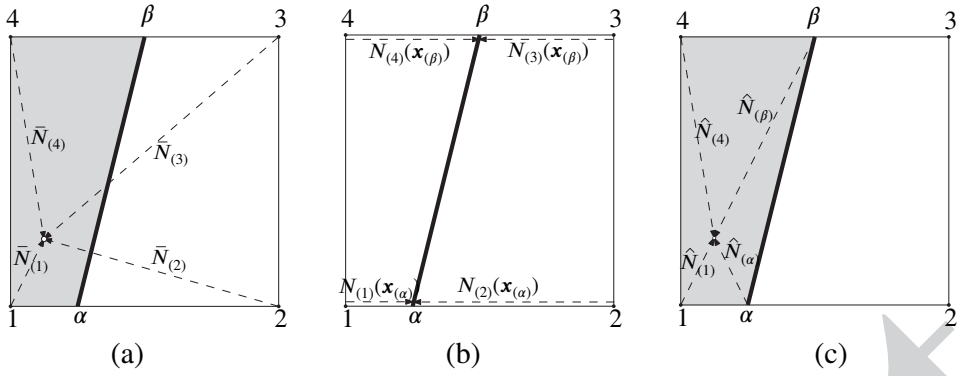

FIGURE 4 Double interpolation: (a) Resulting shape functions ($\bar{\boldsymbol{N}}_{(i)}$). (b) Using shape functions of the original element ($\boldsymbol{N}_{(i)}$) displacements in the intersection points (α , β) are obtained and then (c) From those, displacement at any point of the subdomains are interpolated using shape functions of the sub-domain ($\hat{\boldsymbol{N}}_{(i)}$).

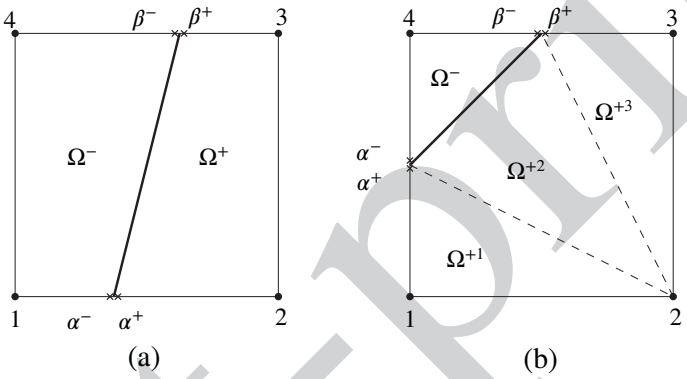

FIGURE 5 (a) "2-2" configuration. (b) "1-3" configuration.

1. The regular interpolation functions $N_{(i)}$ of the original element are used to interpolate the regular and additional displacement values from the original nodes to the points of intersection of the elements edges with the discontinuity line (equations (6)-(7) and Fig. 4 b). This leads to different values of $\boldsymbol{u}$ at points α^- and α^+ (on the left and right of the discontinuity at point α), and β^-, β^+:

$$\boldsymbol{u}^-_{(\alpha)} = \sum_{i\in\Omega^-} N_{(i)}\left(\boldsymbol{x}_{(\alpha)}\right)\boldsymbol{u}_{(i)} + \sum_{i\in\Omega^+} N_{(i)}\left(\boldsymbol{x}_{(\alpha)}\right)\boldsymbol{\delta}_{(i)} \tag{10}$$

$$\boldsymbol{u}^+_{(\alpha)} = \sum_{i\in\Omega^-} N_{(i)}\left(\boldsymbol{x}_{(\alpha)}\right)\boldsymbol{\delta}_{(i)} + \sum_{i\in\Omega^+} N_{(i)}\left(\boldsymbol{x}_{(\alpha)}\right)\boldsymbol{u}_{(i)} \tag{11}$$

$$\boldsymbol{u}^-_{(\beta)} = \sum_{i\in\Omega^-} N_{(i)}\left(\boldsymbol{x}_{(\beta)}\right)\boldsymbol{u}_{(i)} + \sum_{i\in\Omega^+} N_{(i)}\left(\left(\boldsymbol{x}_{(\beta)}\right)\boldsymbol{\delta}_{(i)}\right. \tag{12}$$

$$\boldsymbol{u}^+_{(\beta)} = \sum_{i\in\Omega^-} N_{(i)}\left(\left(\boldsymbol{x}_{(\beta)}\right)\boldsymbol{\delta}_{(i)} + \sum_{i\in\Omega^+} N_{(i)}\left(\left(\boldsymbol{x}_{(\beta)}\right)\boldsymbol{u}_{(i)}\right. \right. \tag{13}$$

2. The values of the function at those points are interpolated again ("sub-interpolated") to the interior of the sub-elements using additional regular linear interpolation functions $\hat{N}_{(i)}$ defined over the continuum sub-elements on the minus (−) and on the plus (+) sides of the original element in terms of local coordinates for each of those subdomains, $\boldsymbol{x}^-$ and $\boldsymbol{x}^+$ (Fig. 4 c):

$$\boldsymbol{u}\left(\boldsymbol{x}^-\right) = \sum_{i\in\Omega^-} \hat{N}_{(i)}\left(\boldsymbol{x}^-\right)\boldsymbol{u}_{(i)} + \sum_{\lambda\in\alpha,\beta} \hat{N}_{(\lambda)}\left(\boldsymbol{x}^-\right)\boldsymbol{u}^-_{(\lambda)} \tag{14}$$

$$\boldsymbol{u}\left(\boldsymbol{x}^{+}\right)=\sum_{\lambda\in\alpha,\beta}\hat{N}_{(\lambda)}\left(\boldsymbol{x}^{+}\right)\boldsymbol{u}_{(\lambda)}^{+}+\sum_{i\in\Omega^{+}}\hat{N}_{(i)}\left(\boldsymbol{x}^{+}\right)\boldsymbol{u}_{(i)} \tag{15}$$

For the purpose of the Finite Element formulation in the following sections, it is convenient to express the above relations in matrix form. The displacement field at any point in the interior of the negative part of the element may be expressed as:

$$\boldsymbol{u}\left(\boldsymbol{x}^{-}\right)=\hat{\mathbf{N}}^{-}\boldsymbol{u}_{e}^{-} \tag{16}$$

where $\hat{\mathbf{N}}^{-}$ is the matrix of shape functions for the interpolation within the negative part of the element, and $\boldsymbol{u}_{e}^{-}$ is the vector of values of displacement at the corners of the negative part of the element. Those corners include the nodes of the negative part of the element and also the intersection points α, β, which may be in turn expressed in terms of the original nodal values. Therefore, $\boldsymbol{u}_{e}^{-}$ may be in turn expressed as:

$$\boldsymbol{u}_{e}^{-}=\mathbf{T}^{-}\bar{\boldsymbol{u}}_{e} \tag{17}$$

where $\mathbf{T}^{-}$ is a matrix containing the original shape functions of the overall element, and $\bar{\boldsymbol{u}}_{e}$ includes all displacement variables of the original element, that is, the regular $\boldsymbol{u}_{(i)}$ as well as the additional $\boldsymbol{\delta}_{(i)}$ nodal displacements, $\bar{\boldsymbol{u}}_{e}=\left(\boldsymbol{u}_{e}\ \boldsymbol{\delta}_{e}\right)^{T}$. Replacing this equation in the previous one,

$$\boldsymbol{u}\left(\boldsymbol{x}^{-}\right)=\hat{\mathbf{N}}^{-}\mathbf{T}^{-}\bar{\boldsymbol{u}}_{e}=\bar{\mathbf{N}}^{-}\bar{\boldsymbol{u}}_{e} \tag{18}$$

where $\bar{\mathbf{N}}^{(-)}$ is the final interpolation matrix for the negative side of the element (Fig. 4 a):

$$\bar{\mathbf{N}}^{-}=\hat{\mathbf{N}}^{-}\mathbf{T}^{-} \tag{19}$$

In the same way, similar equations may be obtained for the positive part:

$$\boldsymbol{u}\left(\boldsymbol{x}^{+}\right)=\hat{\mathbf{N}}^{+}\mathbf{T}^{+}\bar{\boldsymbol{u}}_{e}=\bar{\mathbf{N}}^{+}\bar{\boldsymbol{u}}_{e} \tag{20}$$

with

$$\bar{\mathbf{N}}^{+}=\hat{\mathbf{N}}^{+}\mathbf{T}^{+} \tag{21}$$

The specific format and content of the interpolation matrices will depend on the type of element (e.g. quadrangular, triangular) and the type of intersection scheme with the discontinuity (e.g. “2-2”, “1-3”, etc). For linear quadrangular elements these matrices are specified in Appendix A. Note that since $\bar{\boldsymbol{u}}_{e}$ is composed of the two parts $\boldsymbol{u}_{e}$ and $\boldsymbol{\delta}_{e}$, matrices $\bar{\mathbf{N}}^{-}$, $\bar{\mathbf{N}}^{+}$ can be also decomposed into two parts, $\bar{\mathbf{N}}^{-}=[\bar{\mathbf{N}}_{u}^{-}|\bar{\mathbf{N}}_{\delta}^{-}]$ and $\bar{\mathbf{N}}^{+}=[\bar{\mathbf{N}}_{u}^{+}|\bar{\mathbf{N}}_{\delta}^{+}]$.

2.4 | Matrices B and stiffness matrix K

Knowing the displacement field via equations (18-21), the strain field in the continuum part of the element can be calculated as the derivative of displacements

$$\boldsymbol{\varepsilon}=\mathbf{L}\boldsymbol{u}(x),\quad \boldsymbol{\varepsilon}=\left(\varepsilon_{x}\ \varepsilon_{y}\ \varepsilon_{xy}\right)^{T},\quad \textit{and}\ \ \mathbf{L}=\begin{bmatrix}\partial/\partial x & 0\\ 0 & \partial/\partial y\\ \partial/\partial y & \partial/\partial x\end{bmatrix} \tag{22}$$

Specifying the displacement field for the positive and negative parts of the element, one obtains matrices $\bar{\mathbf{B}}^{-}$ and $\bar{\mathbf{B}}^{+}$:

$$\boldsymbol{\varepsilon}\left(\boldsymbol{x}^{-}\right)=\mathbf{L}\cdot\bar{\mathbf{N}}^{-}\bar{\boldsymbol{u}}_{e}=\bar{\mathbf{B}}^{-}\bar{\boldsymbol{u}}_{e} \tag{23}$$

$$\boldsymbol{\varepsilon}\left(\boldsymbol{x}^{+}\right)=\mathbf{L}\cdot\bar{\mathbf{N}}^{+}\bar{\boldsymbol{u}}_{e}=\bar{\mathbf{B}}^{+}\bar{\boldsymbol{u}}_{e} \tag{24}$$

where matrices $\bar{\mathbf{B}}$, same as $\bar{\mathbf{N}}$, can be decomposed in “u” and “δ” parts:

$$\bar{\mathbf{B}}^{-}=\left[\bar{\mathbf{B}}_{u}^{-}|\ \bar{\mathbf{B}}_{\delta}^{-}\right],\ \bar{\mathbf{B}}_{u}^{-}=\mathbf{L}\cdot\bar{\mathbf{N}}_{u}^{-},\ \bar{\mathbf{B}}_{\delta}^{-}=\mathbf{L}\cdot\bar{\mathbf{N}}_{\delta}^{-} \tag{25}$$

$$\bar{\mathbf{B}}^{+}=\left[\bar{\mathbf{B}}_{u}^{+}|\ \bar{\mathbf{B}}_{\delta}^{+}\right],\ \bar{\mathbf{B}}_{u}^{+}=\mathbf{L}\cdot\bar{\mathbf{N}}_{u}^{+},\ \bar{\mathbf{B}}_{\delta}^{+}=\mathbf{L}\cdot\bar{\mathbf{N}}_{\delta}^{+} \tag{26}$$

Note that, same as for the corresponding matrices **N** matrices, the specific components of $\bar{\mathbf{B}}_u^-$, $\bar{\mathbf{B}}_\delta^-$, $\bar{\mathbf{B}}_u^+$ and $\bar{\mathbf{B}}_\delta^+$ will vary depending on the type of element and intersection considered.

Onto the discontinuity itself, the role of strain in the constitutive laws is played by the normal and tangential relative displacements, grouped here in vector $\boldsymbol{\varepsilon}^J = \left(u_n, u_t\right)^T$. These relative displacements may by obtained by simple matrix arrangement and rotation of the x, y relative displacements $\boldsymbol{a}$ obtained previously in eq. (9):

$$\boldsymbol{\varepsilon}^J = \mathbf{R}\boldsymbol{a} = \mathbf{R}\bar{\mathbf{N}}^J \bar{\boldsymbol{u}}_e = \bar{\mathbf{B}}^J \bar{\boldsymbol{u}}_e \ , \ \bar{\mathbf{B}}^J = \mathbf{R} \cdot \bar{\mathbf{N}}^J \tag{27}$$

Continuum stresses σ are related to strains by the constitutive law, which for the purpose of deriving the stiffness matrix and initial force vectors of the finite element, are assumed to have a general linear format:

$$\boldsymbol{\sigma} = \mathbf{D}\boldsymbol{\varepsilon} + \boldsymbol{\sigma}_0 \tag{28}$$

where the initial stress term may account for stress-free deformations such as thermal, chemical or other swelling effects $\left(\sigma_0 = -D_0\varepsilon_0\right)$ or, in the more general context of the iterative solution of non-linear material behavior, σ_0 may be interpreted as a residual (unbalanced) stress (i.e. as the difference between the previously obtained linear solution stress, and the "true" stress that, according to the non-linear constitutive equation, corresponds to the strain also obtained, see Sect.2.5).

Similarly, for the discontinuity, the stress traction vector $\boldsymbol{\sigma}^J = [\sigma, \tau]^T$ is assumed to be related to relative displacements $\boldsymbol{\varepsilon}^J$ via general linear relation.

$$\boldsymbol{\sigma}^J = \mathbf{D}^J \boldsymbol{\varepsilon}^J + \boldsymbol{\sigma}_0^J \tag{29}$$

From here, the derivation of stiffness matrix and initial force vector follows standard FE procedures. The Principle of Virtual Work (PVW) is applied between a virtual system of nodal displacements $\triangle\bar{\boldsymbol{u}}_e^{vir}$ and the associated strains $\triangle\boldsymbol{\varepsilon}^{vir^-}$, $\triangle\boldsymbol{\varepsilon}^{vir^+}$ and $\triangle\boldsymbol{\varepsilon}^{vir^J}$, and the corresponding conjugate forces and stress variables $\bar{\boldsymbol{F}}_e$, $\boldsymbol{\sigma}^-$, $\boldsymbol{\sigma}^+$ and $\boldsymbol{\sigma}^J$.

For XFEM, virtual displacement vector $\left(\bar{\boldsymbol{u}}_e^{vir\,T}\right)$ and force vector $\left(\bar{\boldsymbol{F}}_e^T\right)$ are composed of the two parts that correspond to real and fictitious degrees of freedom:

$$\bar{\boldsymbol{u}}_e^{vir} = \left[\ \boldsymbol{u}_e^{vir\,T} \middle|\ \boldsymbol{\delta}_e^{vir\,T}\ \right]^T, \ \bar{\boldsymbol{F}}_e = \left[\ \boldsymbol{F}_u^T \middle|\ \boldsymbol{F}_\delta^T\ \right]^T \tag{30}$$

The virtual work done by external forces is calculated multiplying nodal virtual displacements by nodal forces.

$$W_{ext} = \left(\boldsymbol{u}_{\mathbf{e}}^{vir}\right)^T \boldsymbol{F}_u + \left(\boldsymbol{\delta}_e^{vir}\right)^T \boldsymbol{F}_\delta = \left(\bar{\boldsymbol{u}}_e^{vir}\right)^T \bar{\boldsymbol{F}}_e \tag{31}$$

The virtual work of internal forces is given by the integral of the corresponding strains multiplied by their conjugate stress.

$$W_{int} = \left(\bar{\boldsymbol{u}}_e^{vir}\right)^T \cdot \left[\int_{\Omega^-} \left(\bar{\mathbf{B}}^-\right)^T \boldsymbol{\sigma}\, \mathrm{dV} + \int_{\Omega^+} \left(\bar{\mathbf{B}}^+\right)^T \boldsymbol{\sigma}\, \mathrm{dV} + \int_L \left(\bar{\mathbf{B}}^J\right)^T \boldsymbol{\sigma}^J\, \mathrm{dL}\right] \tag{32}$$

Imposing that the work of internal and external forces are equivalent , $W_{ext} = W_{int}$, one obtains the weak matrix form of equilibrium for the overall element including the XFEM discontinuity:

$$\bar{\boldsymbol{F}}_e = \int_{\Omega^-} \left(\bar{\mathbf{B}}^-\right)^T \sigma\, \mathrm{dV} + \int_{\Omega^+} \left(\bar{\mathbf{B}}^+\right)^T \sigma\, \mathrm{dV} + \int_L \left(\bar{\mathbf{B}}^J\right)^T \boldsymbol{\sigma}^J\, \mathrm{dL} \tag{33}$$

Note that this format is similar to the traditional FEM expressions, except that it includes the contribution from the negative, positive and discontinuity parts of the element.

Replacing in this equation the stresses with the constitutive laws (Eq.(28) and (29)), and then strains with their expressions in terms of **B** matrices and nodal displacements (eqs. 23, 24 and 27), the typical finite element expression is obtained:

$$\bar{\boldsymbol{F}}_e = \bar{\mathbf{K}}_e \cdot \bar{\boldsymbol{u}}_e + \bar{\boldsymbol{F}}_{e\,0} \tag{34}$$

where

$$\bar{\mathbf{K}}_e = \int_{\Omega^-} \left(\bar{\mathbf{B}}^-\right)^T \mathbf{D}\bar{\mathbf{B}}^- \mathrm{dV} + \int_{\Omega^+} \left(\bar{\mathbf{B}}^+\right)^T \mathbf{D}\bar{\mathbf{B}}^+ \mathrm{dV} + \\ + \int_L \left(\bar{\mathbf{B}}^J\right)^T \mathbf{D}^J \bar{\mathbf{B}}^J \mathrm{dL} \tag{35}$$

$$\bar{\boldsymbol{F}}_{e0} = \int_{\Omega^-} \left(\bar{\mathbf{B}}^-\right)^T \boldsymbol{\sigma}_0 \mathrm{dV} + \int_{\Omega^+} \left(\bar{\mathbf{B}}^+\right)^T \boldsymbol{\sigma}_0 \mathrm{dV} + \int_L \left(\bar{\mathbf{B}}^J\right)^T \boldsymbol{\sigma}_0^J \mathrm{dL} \tag{36}$$

Replacing now XFEM vectors and matrices by their "u" and "δ" parts one can obtain more detailed expressions:

$$\bar{\mathbf{K}}_e = \begin{bmatrix} \bar{\mathbf{K}}_{uu} & \bar{\mathbf{K}}_{u\delta} \\ \bar{\mathbf{K}}_{\delta u} & \bar{\mathbf{K}}_{\delta\delta} \end{bmatrix} \tag{37}$$

where

$$\begin{aligned}
\bar{\mathbf{K}}_{uu} &= \int_{\Omega^-} \left(\bar{\mathbf{B}}_u^-\right)^T \cdot \mathbf{D} \cdot \bar{\mathbf{B}}_u^- \mathrm{dV} + \int_{\Omega^+} \left(\bar{\mathbf{B}}_u^+\right)^T \cdot \mathbf{D} \cdot \bar{\mathbf{B}}_u^+ \mathrm{dV} + \int_L \left(\bar{\mathbf{B}}_u^J\right)^T \cdot \mathbf{D}^J \cdot \bar{\mathbf{B}}_u^J \mathrm{dL} \\
\bar{\mathbf{K}}_{u\delta} &= \int_{\Omega^-} \left(\bar{\mathbf{B}}_u^-\right)^T \cdot \mathbf{D} \cdot \bar{\mathbf{B}}_\delta^- \mathrm{dV} + \int_{\Omega^+} \left(\bar{\mathbf{B}}_u^+\right)^T \cdot \mathbf{D} \cdot \bar{\mathbf{B}}_\delta^+ \mathrm{dV} - \int_L \left(\bar{\mathbf{B}}_u^J\right)^T \cdot \mathbf{D}^J \cdot \bar{\mathbf{B}}_\delta^J \mathrm{dL} \\
\bar{\mathbf{K}}_{\delta u} &= \int_{\Omega^-} \left(\bar{\mathbf{B}}_\delta^-\right)^T \cdot \mathbf{D} \cdot \bar{\mathbf{B}}_u^- \mathrm{dV} + \int_{\Omega^+} \left(\bar{\mathbf{B}}_\delta^+\right)^T \cdot \mathbf{D} \cdot \bar{\mathbf{B}}_u^+ \mathrm{dV} - \int_L \left(\bar{\mathbf{B}}_\delta^J\right)^T \cdot \mathbf{D}^J \cdot \bar{\mathbf{B}}_u^J \mathrm{dL} \\
\bar{\mathbf{K}}_{\delta\delta} &= \int_{\Omega^-} \left(\bar{\mathbf{B}}_\delta^-\right)^T \cdot \mathbf{D} \cdot \bar{\mathbf{B}}_\delta^- \mathrm{dV} + \int_{\Omega^+} \left(\bar{\mathbf{B}}_\delta^+\right)^T \cdot \mathbf{D} \cdot \bar{\mathbf{B}}_\delta^+ \mathrm{dV} + \int_L \left(\bar{\mathbf{B}}_\delta^J\right)^T \cdot \mathbf{D}^J \cdot \bar{\mathbf{B}}_\delta^J \mathrm{dL}
\end{aligned} \tag{38}$$

and

$$\bar{\boldsymbol{F}}_{e0} = \begin{bmatrix} \boldsymbol{F}_{u0} \\ \boldsymbol{F}_{\delta 0} \end{bmatrix} \tag{39}$$

$$\boldsymbol{F}_{u0} = \int_{\Omega^-} \left(\bar{\mathbf{B}}_u^-\right)^T \cdot \boldsymbol{\sigma}_0 \mathrm{dV} + \int_{\Omega^+} \left(\bar{\mathbf{B}}_u^+\right)^T \cdot \boldsymbol{\sigma}_0 \mathrm{dV} + \int_L \left(\bar{\mathbf{B}}_u^J\right)^T \cdot \boldsymbol{\sigma}_0^J \mathrm{dL} \tag{40}$$

$$\boldsymbol{F}_{\delta 0} = \int_{\Omega^-} \left(\bar{\mathbf{B}}_\delta^-\right)^T \cdot \boldsymbol{\sigma}_0 \mathrm{dV} + \int_{\Omega^+} \left(\bar{\mathbf{B}}_\delta^+\right)^T \cdot \boldsymbol{\sigma}_0 \mathrm{dV} - \int_L \left(\bar{\mathbf{B}}_\delta^J\right)^T \cdot \boldsymbol{\sigma}_0^J \mathrm{dL} \tag{41}$$

Note once more, that specific components of these element matrices and vectors will be different for each type of element and intersection, as the consequence of the specific expressions of matrices **N** and **B**.

All previous developments in this section and in Appendix A have been formulated for quadrangular elements, for which double interpolation leads to a formulation which is different from the more common one obtained with natural interpolation. In the case of linear triangles, both formulations turn out equivalent since interpolating linearly along edges to intersection points, and then again linearly into the subdomain, leads to the same result as direct linear interpolation from vertices. Nevertheless, the same type of formulation as just presented for quadrangles is also developed for triangles in Appendix C. This is done for completeness, and also because with this format of equations it is possible to relate the XFEM formulation to the classical FEM with zero-thickness interface elements, as discussed in Sect. 4.

2.5 | Extension to non-linear constitutive behavior of the discontinuity

The formulation described for linear constitutive behavior of the discontinuity may be easyly extended to cover non-linear constitutive behavior using standard iterative FE procedures (e.g.[27]). In that context, and for each iteration, the element stiffness matrix and initial force vector in (34) take the meaning of tangential or algorithmic element stiffness matrix, and residual (or

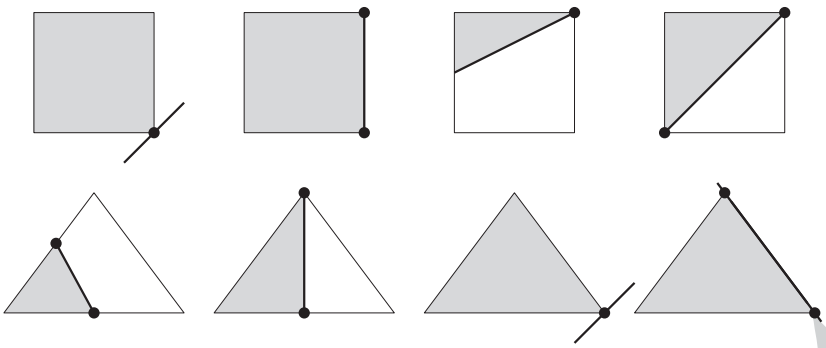

FIGURE 6 Special cases on quadrangular and triangular elements where the discontinuity coincides with nodes or edges.

internal) element force vector, which may be evaluated from constitutive stiffness and residual (or internal) constitutive stresses of the discontinuity, by same expressions (35)-(41).

3 | MOVING NODES TO THE DISCONTINUITY AND SPECIAL CONFIGURATION CASES

As already explained in the Introduction, one of the problems with XFEM (that will be illustrated with an example in section 5) is caused by nodes lying too close to the discontinuity line. In that case, the numerical results tend to produce oscillations. One possible solution to this problem consists of moving the corresponding nodes away from the discontinuity itself (e.g.[26]). However, this may be done in various directions and also requires deciding the magnitude of such displacement. In this paper, the opposite strategy is adopted: to move the affected nodes onto the discontinuity itself. This can be done more easily in a unique way using the perpendicular direction to the discontinuity line (shortest distance). As the consequence, new element-discontinuity configurations are generated in which the discontinuity coincides in one or more nodes of the element. These cases deserve separate treatment and are considered in this section and in Appendices B and C.

For quadrangular elements, it is only necessary to define four types of special cases (Fig. 6) and the rest can be deduced by symmetry or rotation. These configurations are not particular cases of the "2-2" or "1-3 " configurations, because different subdomains are created, in some cases a complete subdomain disappears or changes shape and therefore its interpolation and **T** matrices also change. Particularized formulation for these four cases are developed in Appendix B. Similarly, special cases for triangles are shown in Fig. 6 bottom, also formulated in Appendix C.

4 | EQUIVALENCE BETWEEN XFEM AND ZERO-THICKNESS INTERFACE ELEMENTS

As already suggested in previous sections, thanks to the assumption of the sub-interpolation, it is possible to establish the equivalence between the proposed formulation of XFEM, and a standard FEM formulation with zero-thickness interface elements (FEM+z) in which one standard continuum element is used for each XFEM integration sub-domain, and one zero-thickness interface is used for the discontinuity segment contained in the original element. The equivalence is first demonstrated for the case of the "2-2" discontinuity configuration on the quadrangular element, which is shown in Fig. 7 a assuming a FEM+z formulation, and in Fig. 5 a assuming the proposed XFEM formulation. The case of the "1-3" configuration of the same element is also shown on Fig. 7 b, and is discussed later.

4.1 | "2-2 " configuration

As seen in Fig.7 a, for the traditional FEM+z formulation, the nodal variables would be the displacements of nodes 1 to 8, including the corner nodes 1-4 (same as in the XFEM approach) plus the four nodes 5-8 located on the right and left of each discontinuity at its intersection with the upper and lower domain limits. Comparing to the XFEM formulation, nodes 5, 6, 7 and 8 would correspond to XFEM points α^+, β^+, α^-, β^- respectively (Fig 5 a-7 a). The domain would include two standard quadrangular elements, one with nodes 1, 7, 8 and 4 (corresponding to XFEM subdomain Ω^- with corner points 1, α^-, β^- and

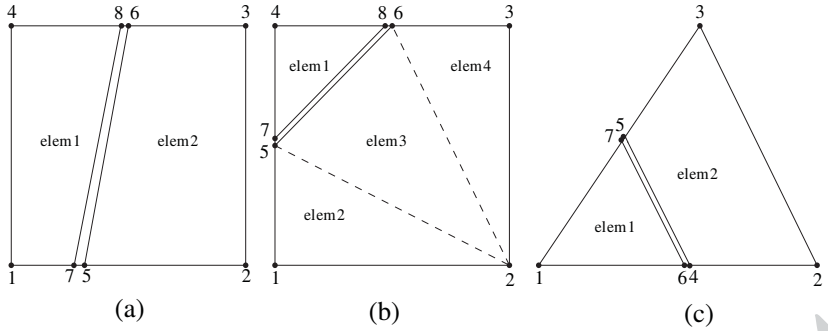

FIGURE 7 (a) Element with"2-2 " discontinuity configuration in the context of FEM+z formulation. (b) Same with "1-3 " discontinuity configuration. (c) Same with triangular element configuration.

4) and the second with nodes 5, 2, 3 and 6 (corresponding to subdomain Ω^+ with corner points α^+, 2 and β^+). The interface element would connect nodes 5, 6, 7 and 8, that is XFEM points α^+, β^+, α^- and β^-. The stiffness matrices of those elements would have expressions:

$$\hat{\mathbf{K}}^{e1}=\int_{e1}\left(\hat{\mathbf{B}}^{e1}\right)^T\mathbf{D}\hat{\mathbf{B}}^{e1}\mathrm{dV},\ \hat{\mathbf{K}}^{e2}=\int_{e2}\left(\hat{\mathbf{B}}^{e2}\right)^T\mathbf{D}\hat{\mathbf{B}}^{e2}\mathrm{dV},\ \hat{\mathbf{K}}^{eJ}=\int_{eJ}\left(\hat{\mathbf{B}}^{eJ}\right)^T\mathbf{D}\hat{\mathbf{B}}^{eJ}\mathrm{dL} \tag{42}$$

Where $\hat{\mathbf{B}}^{e1}$, $\hat{\mathbf{B}}^{e2}$ are the standard FEM matrices obtained as $\hat{\mathbf{B}}^{e1}=\mathbf{L}\hat{\mathbf{N}}^{e1}$ and $\hat{\mathbf{B}}^{e2}=\mathbf{L}\hat{\mathbf{N}}^{e2}$, being $\hat{\mathbf{N}}^{e1}$ and $\hat{\mathbf{N}}^{e2}$ the same local interpolation matrices defined as $\hat{\mathbf{N}}^-$ and $\hat{\mathbf{N}}^+$ in (A3) and (A9). Matrix $\hat{\mathbf{B}}^J$ is the standard interface element matrix obtained as $\hat{\mathbf{B}}^{eJ}=\mathbf{R}\hat{\mathbf{N}}^{eJ}$, being $\hat{\mathbf{N}}^{eJ}$ the same matrix defined in (23).

Going back now to the expression of the overall element XFEM stiffness matrix (35), by replacing continuum $\mathbf{B}$ matrices as the product of $\mathbf{L}$ and $\bar{\mathbf{N}}$, equations (23-24), replacing interface $\mathbf{B}$ matrix as the product $\mathbf{R}\bar{\mathbf{N}}$, equation (27), and finally all $\bar{\mathbf{N}}$ matrices as the products of the respective $\hat{\mathbf{N}}$ and $\mathbf{T}$ matrices, equations (19), (21) and (A17), that expression may be rewritten as:

$$\bar{\mathbf{K}}_e=\bar{\mathbf{K}}^-+\bar{\mathbf{K}}^+\bar{\mathbf{K}}^J \tag{43}$$

where

$$\bar{\mathbf{K}}^-=\int_{\Omega^-}\left(\bar{\mathbf{B}}^-\right)^T\mathbf{D}\bar{\mathbf{B}}^-\mathrm{d}\Omega=\left(\mathbf{T}^-\right)^T\left(\int_{\Omega^-}\left(\hat{\mathbf{B}}^-\right)^T\mathbf{D}\hat{\mathbf{B}}^-\mathrm{d}\Omega\right)\mathbf{T}^- \tag{44}$$

$$\bar{\mathbf{K}}^+=\int_{\Omega^+}\left(\bar{\mathbf{B}}^+\right)^T\mathbf{D}\bar{\mathbf{B}}^+\mathrm{d}\Omega=\left(\mathbf{T}^+\right)^T\left(\int_{\Omega^+}\left(\hat{\mathbf{B}}^+\right)^T\mathbf{D}\hat{\mathbf{B}}^+\mathrm{d}\Omega\right)\mathbf{T}^+ \tag{45}$$

$$\bar{\mathbf{K}}^J=\int_L\left(\bar{\mathbf{B}}^J\right)^T\mathbf{D}^J\bar{\mathbf{B}}^J\mathrm{dL}=\left(\mathbf{T}^J\right)^T\left(\int_L\left(\hat{\mathbf{B}}^J\right)^T\mathbf{D}^J\hat{\mathbf{B}}^J\mathrm{dL}\right)\mathbf{T}^J \tag{46}$$

and

$$\hat{\mathbf{B}}^-=\mathbf{L}\hat{\mathbf{N}}^-,\quad \hat{\mathbf{B}}^+=\mathbf{L}\hat{\mathbf{N}}^+,\quad \hat{\mathbf{B}}^J=\mathbf{R}\hat{\mathbf{N}}^J, \tag{47}$$

which finally leads to:

$$\bar{\mathbf{K}}_e=\left(\mathbf{T}^-\right)^T\hat{\mathbf{K}}_e^-\mathbf{T}^-+\left(\mathbf{T}^+\right)^T\hat{\mathbf{K}}_e^+\mathbf{T}^+\left(\mathbf{T}^J\right)^T\hat{\mathbf{K}}_e^J\mathbf{T}^J \tag{48}$$

Since matrices $\hat{\mathbf{N}}$ and $\hat{\mathbf{B}}$ for the $^-$, $^+$ and ^{J} contributions to the XFEM stiffness, as well as the respective domains of integration, are the same as those for elements 1, 2 and J of the standard FEM formulation, respectively, the resulting local stiffness matrices $\hat{\mathbf{K}}$ will also be identical, that is:

$$\hat{\mathbf{K}}^{e1}=\hat{\mathbf{K}}^-,\ \hat{\mathbf{K}}^{e2}=\hat{\mathbf{K}}^+,\ \hat{\mathbf{K}}^{eJ}=\hat{\mathbf{K}}^J \tag{49}$$

The remaining aspect would refer to the product with **T** matrices in (48). However, this aspect may be trivial since the **T** matrices may be interpreted as the transport assembly matrices to relocate the contributions of each local stiffness matrix in the overall stiffness matrix. In this way, each $\mathbf{T}^T\hat{\mathbf{K}}\mathbf{T}$ product turns out to be a global stiffness matrix with the only non-zero terms corresponding to the $\hat{\mathbf{K}}$ matrix considered, and summation of the three of them leads to the overall stiffness matrix for the XFEM element including discontinuity.

A similar expression to (49) could be written for the FEM+z formulation using the corresponding T matrices, which would be different from the ones above, since the overall displacement vector does not contain the same variables ($\boldsymbol{u}_{(1)}...\boldsymbol{u}_{(4)}$, $\boldsymbol{u}_{(5)}...\boldsymbol{u}_{(8)}$ for FEM+z, instead of $\boldsymbol{u}_{(1)}...\boldsymbol{u}_{(4)}$, $\boldsymbol{\delta}_{(1)}...\boldsymbol{\delta}_{(4)}$ for XFEM). However, one could consider the FEM+z formulation with a change of variables such that variables $\boldsymbol{u}_{(5)}...\boldsymbol{u}_{(8)}$ would be exchanged by $\boldsymbol{\delta}_{(1)}...\boldsymbol{\delta}_{(4)}$. That can be done easily using linear functions between node 1 and 2 for instance, and $\boldsymbol{\delta}_{(2)}$ would be the result of linear extrapolation of the straight function defined by $\boldsymbol{u}_{(1)}$ and $\boldsymbol{u}_{(7)}$ along the bottom side, or conversely, $\boldsymbol{u}_{(7)}$ would be the linear interpolation between values $\boldsymbol{u}_{(1)}$ and $\boldsymbol{\delta}_{(2)}$. And this is exactly the content of the $\mathbf{T}^-$, $\mathbf{T}^+$ and $\mathbf{T}^J$. Therefore, eq. (48) can be reinterpreted as the assembly of the FEM+z element matrices in the system of variables used in the XFEM formulation, which proves the full equivalence of XFEM formulation with double interpolation, with the traditional FEM+z formulation in the case of quadrangular elements with "2-2"discontinuity configuration.

4.2 | "1-3 " configuration

Fig. 7 b shows the FEM+z mesh for the XFEM quadrangular element with "1-3" configuration of discontinuity intersection, Fig. 5 b. The FEM+z mesh contains four triangles $e1$, $e2$, $e3$ and $e4$, that correspond to the four integration subdomains Ω^-, Ω^{+1}, Ω^{+2}, and Ω^{+3}, and one interface element eJ that corresponds to the discontinuity contribution ^{J}.

By similar reasoning as before, one can easily conclude that the five local stiffness matrices $\hat{\mathbf{K}}$ will be the same for both, FEM+z and XFEM. However, the assembly here turns out a little trickier. In the previous "2-2" configuration the exchange of variables was one-to-one, and was invertible, that is, the four "$\boldsymbol{u}$" displacements ($\boldsymbol{u}_{(5)}...\boldsymbol{u}_{(8)}$) of the interface nodes where exchanged by the four "$\boldsymbol{\delta}$" nodal overhang displacements of the XFEM formulation. Therefore the final system had the same number of independent variables.

However, in the present configuration, the number of variables decreases because the original four nodal displacements $\boldsymbol{u}_{(5)}...\boldsymbol{u}_{(8)}$ (that in the FEM+z formulation do not change from previous configuration), in the case of XFEM are reduced to only three, specifically to $\boldsymbol{\delta}_{(1)}$, $\boldsymbol{\delta}_{(3)}$ and $\boldsymbol{\delta}_{(4)}$ (while $\boldsymbol{\delta}_{(2)}$, although formally present, does not participate in the system).

This may be intuitively explained because the $\boldsymbol{u}$ and $\boldsymbol{\delta}$ values of corner nodes 1 and 4 participate in the linear interpolation of the displacements of interface nodes 5 and 7, and those of nodes 3 and 4 participate for nodes 6 and 8, but node 2 does not participate in either of them. This is reflected by empty columns corresponding to $\boldsymbol{\delta}_{(2)}$ in all the corresponding **T** matrices given in equations (A22), (A28), (A34), (A40) of Appendix A. Which means that no stiffness term will be assembled to the corresponding global row/column in this configuration.

Aside from practical computational problems that can be circumvented (e.g. after assembly those "inactive" $\boldsymbol{\delta}$ variables have to be identified and their values prescribed to avoid zero pivot in the solution), the mechanical effect is that the XFEM formulation has fewer independent degrees of freedom, that is, it is kinematically restricted with respect to the same mesh solved using the traditional FEM+z formulation. This means that one can expect the solution of the same physical problem using XFEM to exhibit lower accuracy (and perhaps oscillations) as compared to the one obtained using the FEM+z approach.

4.3 | Triangular elements and special configurations

In the case of triangular elements (formulation developed in Appendix C) similar reasoning leads to the conclusion that in the general case (Fig.C2 a) the XFEM formulation is always equivalent to a kinematically restricted version of the FEM+z formulation applied to the same mesh. This is easily verified by a simple variable count, since FEM+z would lead to seven nodes while XFEM leads to the number of variables equivalent to six nodes.

However, a remarkable observation is that the above conclusions (for both quadrangles and triangles) are only valid for the general intersection case in which the discontinuity does not coincide with nodes or edges. Indeed, in the special cases that intersection does coincide with nodes or edges (Fig.B1 a to e in Appendix B), it can be easily verified that the count changes and equivalence exists again between XFEM and FEM+z formulations (e.g. in cases of Fig. B1 a, B1 c, B1 d and B1 e, the number of nodes in FEM+z would be seven, six, five and six, respectively, and the number of independent variables equivalent

in XFEM too). Similarly for triangles, the number of nodes in FEM+z for especial configurations in Fig. C2 b, C2 c, and C2 d in Appendix C would be six, four and five, and also the total number of variables equivalent in XFEM.

For this reason, it should not be surprising that the proposed strategy of moving close nodes onto the discontinuity itself is not only numerically convenient because it eliminates small subdomains, but also because it leads to configurations that maximize the number of independent degrees of freedom. This beneficial effect will be shown in some of the Examples (Sect.5).

5 | EXAMPLE SIMULATIONS

This section includes three numerical examples, including a beam bending problem and the stress distribution around a tunnel, both with linear-elastic behavior of the discontinuity, as well as uniaxial compression specimen with an inclined discontinuity sliding under shear-compression.

5.1 | Elastic beam bending

The first example consists of a cantilever beam subject to a vertical load at its end, as represented in Fig. 8 . The material is linear elastic, isotropic and homogeneous, and plane stress behavior is assumed. The elastic solution is given by beam theory, with linear distribution of normal stress and parabolic distribution of shear stress on vertical cross-sections perpendicular to the beam axis. This example was also used in previous XFEM papers such as[24], and therefore it can be compared to both analytical solution and to numerical results. The beam dimensions are 16m of length and 4m width ($L = 16$m, $c = 2$m) and material properties for the continuum elements are Young modulus $E = 1000$MPa and Poisson's ratio $\nu = 0.3$.

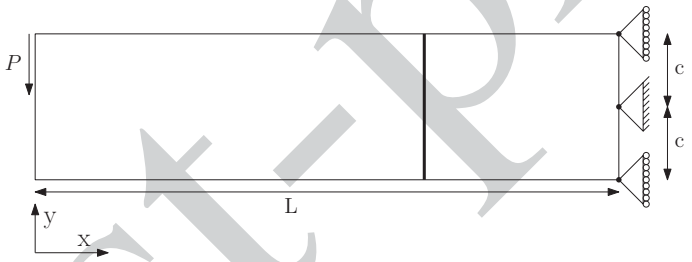

FIGURE 8 Geometry for beam bending test problem.

The stress boundary conditions are imposed on the right and left ends of the beam. The vertical load on the left end is $P = -1$MN, and is distributed on the nodes of that cross-section according to a parabolic distribution as given by beam theory. On the right-hand side, the same parabolic distribution is applied but with the opposite sign. Right top and bottom nodes are constrained in x-direction and the central node is constrained (Fig. 8). The distributed forces applied on both (left and right) vertical cross-sections are given by the following expressions:

$$\begin{cases} f_x(0,y) & = 0 \\ f_y(0,y) & = \frac{P}{2I}\left(c^2 - y^2\right) \\ f_x(L,y) & = \frac{PLy}{I} \\ f_y(L,y) & = -\frac{P}{2I}\left(c^2 - y^2\right) \end{cases} \tag{50}$$

where I is the inertia moment: $I = (2c)^3/12$.

Additionally, a vertical discontinuity is assumed located at the cross-section at $x = 11$m. Its behavior is assumed linear elastic with high stiffness values, so that it does not add any deformability, and therefore the beam behavior should be equivalent to the behavior given by beam theory (that is, without discontinuity), Eq.(51),

$$\begin{cases} \sigma_{xx} & = -\frac{Pxy}{I} \\ \sigma_{xy} & = \frac{P}{2I}\left(c^2 - y^2\right) \end{cases} \tag{51}$$

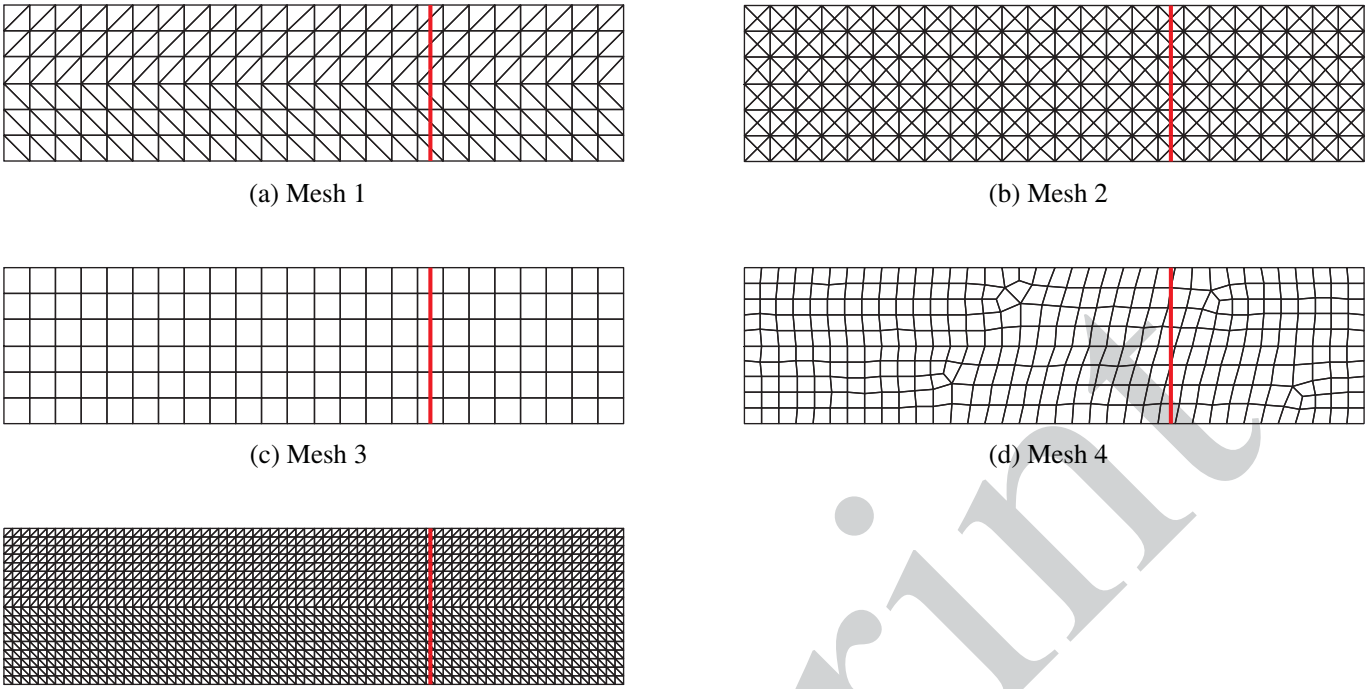

(a) Mesh 1

(b) Mesh 2

(c) Mesh 3

(d) Mesh 4

(e) Mesh 5

FIGURE 9 Meshes used to discretize the Cantilever beam of example two: (a) Biased structured triangular mesh with 12 elements across the beam depth. (b) Unbiased structured triangular mesh with 12 elements across the beam depth. (c) Structured quadrangular mesh with 6 elements across the beam depth (d) Unstructured quadrangular mesh with 10 elements across the beam depth, some of them really close to the discontinuity line (e) Structured triangular mesh with 36 elements across the beam depth (it is a refinement 1/3 of Mesh 1).

For the analysis, the beam has been discretized with various meshes, as shown in Fig. 9 . The calculations have been run with two values of discontinuity stiffness, $K_N = K_T = 9000$MPa/m (same as in[24]) and a much higher value $K_N = K_T = 10^7$MPa/m (K_N, K_T are the main diagonal components of the interface elastic stiffness $\mathbf{D}^J$ in eq.29, which has been assumed with a diagonal format).

The first results presented are the comparison with the results from[24], specifically with the penalty formulation in that paper, using similar mesh and parameter values, that is, with the dense triangular Mesh 5 (Fig. 9 e) and discontinuity stiffness $K_N = K_T = 9000$MPa/m. The results obtained are shown in Fig. 10 in terms of normal and shear stresses on the discontinuity cross-section, together with the predictions by beam formulas and the corresponding results from[24]. As seen, there is very good match with Sander's results, something that could be expected given the equivalence of the formulations used (as explained in Sect. **??** in the case of triangles the proposed formulation coincides with the usual XFEM formulation based on natural interpolation, and also the linear elastic assumption for the discontinuity should be equivalent to the penalty formulation in[24]).

The results obtained with meshes 1 to 4, and with $K_N = K_T = 9000$MPa/m and $K_N = K_T = 10^7$MPa/m, are shown in Figures 11 and 12 .

Fig. 11 shows the results obtained with triangular meshes 1 and 2 (Fig. 9 a and 9 b), and Fig. 12 shows the results obtained with quadrangular elements, meshes 3 and 4 (Fig. 9 c and 9 d).

As seen in Fig. 11 , XFEM calculations using linear triangles with "biased" orientation seem very sensitive to the discontinuity stiffness (penalty) values of K_N, K_T; the results obtained with the low density mesh 1 with the value $K_N = K_T = 9000$MPa/m (same as used in[24]) already show some oscillations, but if that value is increased in three orders of magnitude to $K_N = K_T = 10^7$MPa, oscillations become much larger, clearly excessive. On the other hand, mesh 2 is also made of linear triangles with similar density, but using an unbiased more symmetric arrangement, and the discontinuity is made to coincide with a line of "central" nodes to each mesh cell. In that case, the solution is much smoother and becomes insensitive to higher stiffness values.

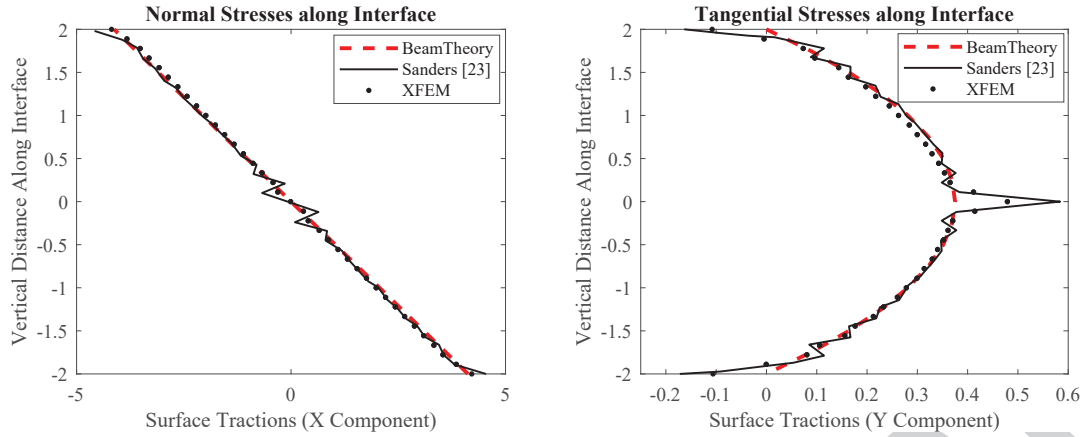

FIGURE 10 Interface tractions for XFEM discontinuity, together with analytical solution by beam theory, and results from[24].

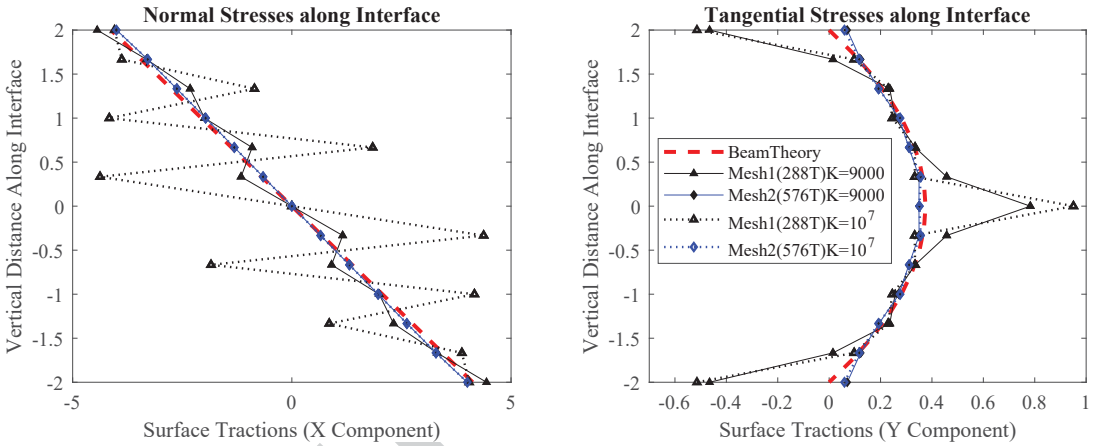

FIGURE 11 Normal and tangential stress distribution along the discontinuity using triangular elements.

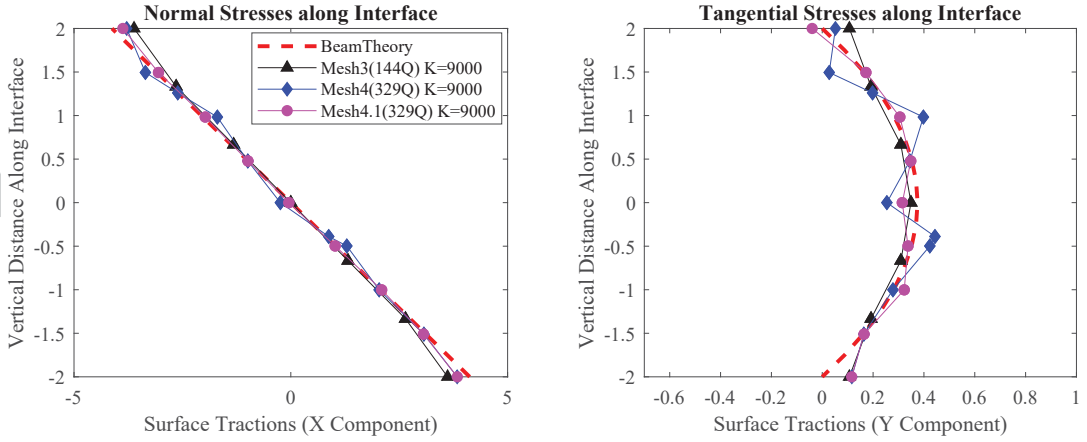

FIGURE 12 Normal and tangential stress distribution along the discontinuity using quadrangular elements and $K_N = K_T =$ 9000MPa/m.

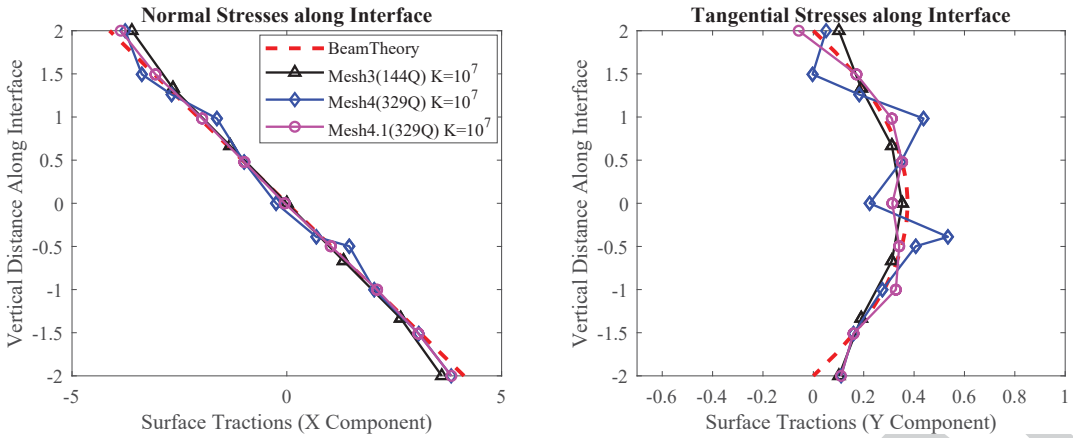

FIGURE 13 Normal and tangential stress distribution along the discontinuity using quadrangular elements and $K_N = K_T = 10^7$MPa/m.

In Fig. 12 , the results for quadrangular meshes 3 and 4 are depicted. Mesh 3 is a regular mesh with discontinuity intersecting elements in a very favorable way, which shows very accurate smooth results. Mesh 4 is a random mesh of similar density, in which some nodes happen to fall very close to the discontinuity line. This is reflected in some oscillations observed in the results for that mesh. Mesh 4.1, also listed in Fig.12 , is very similar to Mesh 4 with the only difference that the nodes closest to the discontinuity have been moved onto the discontinuity itself (strategy proposed in this paper to remedy this situation). As seen in the results, this strategy really succeeds in eliminating the oscillations. Also to be mentioned, all results for quadrangular elements seem much less sensitive (or not sensitive at all) to the increase of stiffness coefficient in three orders of magnitude from 9000 to 10^7MPa/m, and similar accuracies are obtained with much lower density of elements as compared to linear triangles, provided the strategy of moving close nodes the discontinuity itself is applied.

5.2 | Tunnel cross-section

The second example consists of a tunnel of 6m radius in the center of a square 120 × 120m domain with a distributed load of 8MPa on the top, 4MPa on the right side and prescribed normal displacements on bottom and left boundaries (Fig. 14). A XFEM radial discontinuity with high elastic stiffness is also considered, which will allow us to evaluate normal and shear stresses along this line and compare them to the theoretical values given by the Kirsch solution ([28]).

Elastic parameters for the continuum are $E = 100$MPa and $\nu = 0.3$. Normal and shear elastic stiffness values for the discontinuity are $K_N = 10^8$MPa/m and $K_T = 10^8$MPa/m. This case has been solved with a random quadrangular mesh as discussed in the following paragraphs.

The mesh considered is shown in Fig. 15 a, consisting of 920 quadrangular elements, 25 of which are crossed by the XFEM discontinuity.

Fig. 16 shows the normal and shear stress distribution along the discontinuity line (dots) together with the closed-form solution (continuous line). It can be seen that the XFEM results are in general very close to the analytical solution except near the section around $x \simeq 18$m where some oscillating values are observed. Analyzing it in detail, the highest oscillation corresponds to elements where the discontinuity lies very close to a node (Fig. 15 b).

As explained in the introduction and in Section 3, the proposed strategy in these cases is to move the closest nodes onto the discontinuity itself, obtaining in this way the special type of element configuration described in Section 3. The efficiency of this technique is demonstrated again in this case, since its application leads to the new results also shown in Fig. 16 , in which oscillations have disappeared.

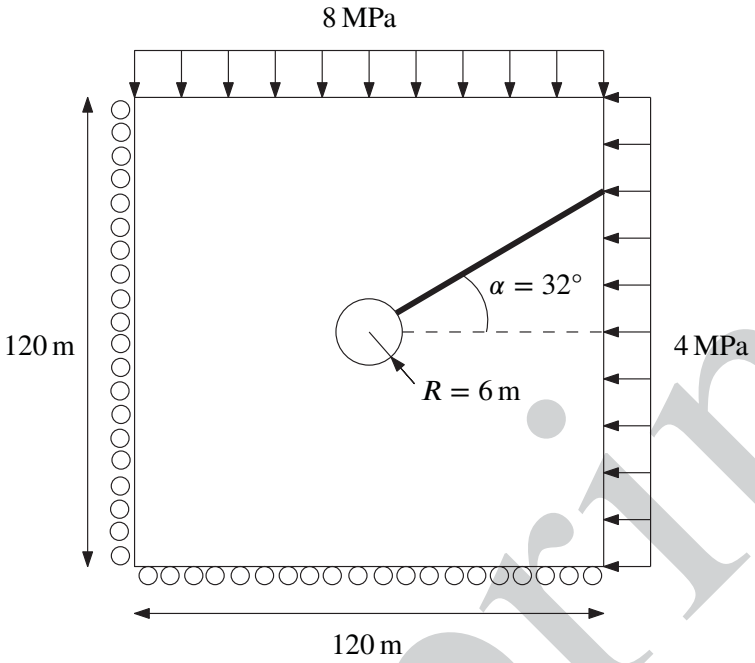

FIGURE 14 Geometry for the tunnel test problem of example 3.

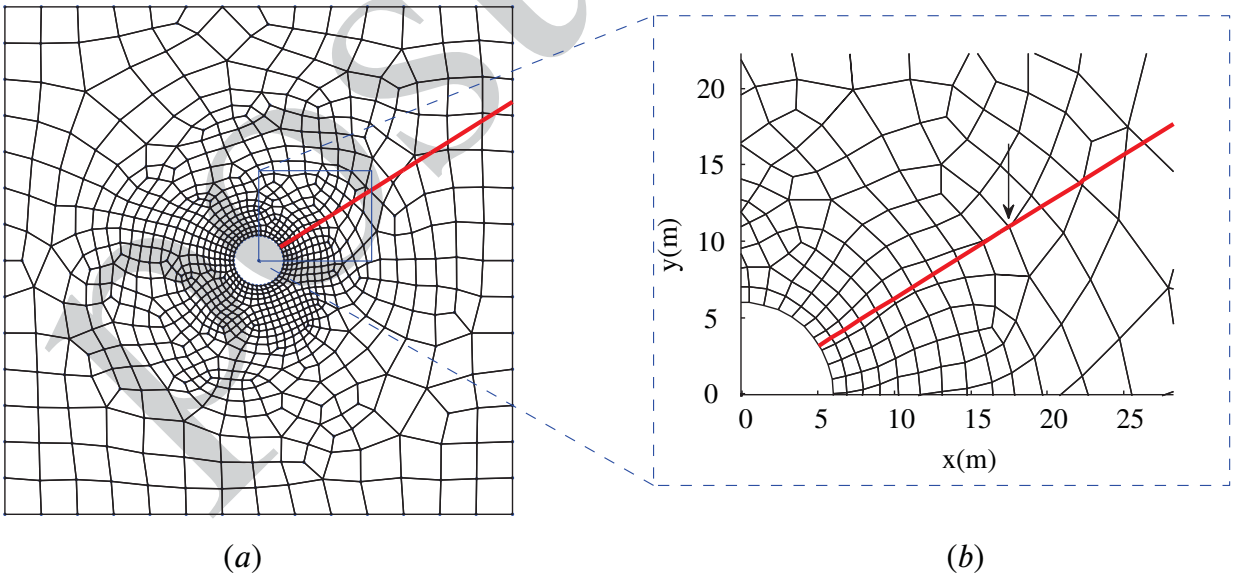

FIGURE 15 (a) Unstructured quadrangular mesh with 920 elements 25 of which are crossed by the discontinuity with configurations "2-2 " and "1-3 ". (b) Mesh detail to show the nodes closest to discontinuity line.

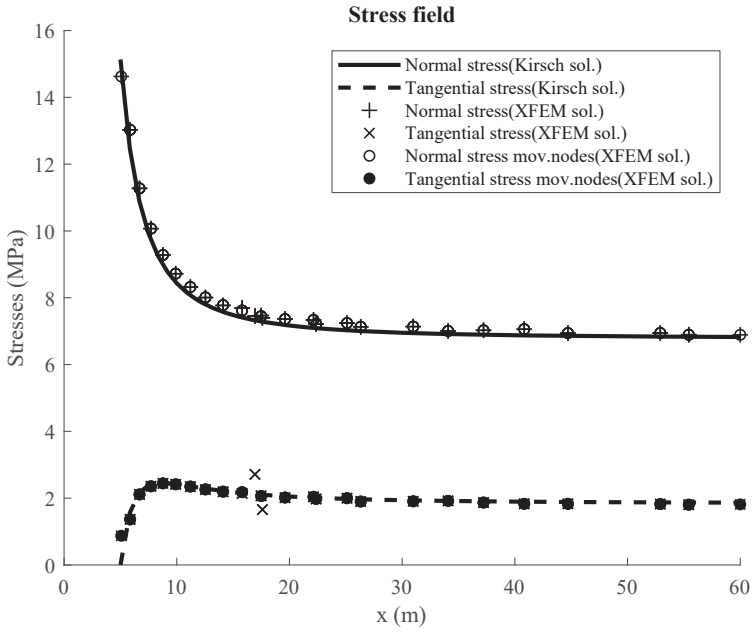

FIGURE 16 Numerical results for mesh of Fig. 15 moving closest nodes onto the discontinuity itself (Note +/× symbols for original results).

5.3 | Compression test with non-linear constitutive law on the discontinuity

The proposed formulation can be also used to solve non linear problems. This schematic example consists of a rectangular specimen of two elements, one of them crossed by an inclined discontinuity (Figure 17), which incorporates a fracture mechanics-based elastoplastic constitutive model described in[5]. This model is based on a hyperbolic loading function depending on three parameters χ (tensile strength), c (apparent cohesion) and $\tan\phi$ (asymptotic friction angle), the evolution of which depends on the work spent during the fracture process W^{cr} (softening). The softening laws are such that tensile strength vanishes when W^{cr} reaches the fracture energy in mode I G_f^I, and apparent cohesion vanishes later, when W^{cr} reaches a second fracture energy for shear compression, G_f^{IIa}, generally larger than G_f^I (G_f^I and G_f^{IIa} are two of the model parameters).

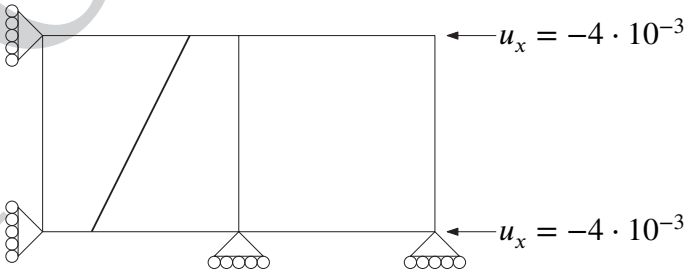

FIGURE 17 Geometry for compression specimen example.

The values assumed for material properties are Young modulus of $\cdot 10^6$MPa and Poisson's ratio $\nu = 0.1$ for the continuum. For the discontinuity, parameters are: normal and tangential stiffness coefficients $K_N = K_T = 10^{10}$MPa/m, apparent or asymptotic cohesion ($c = 40$MPa), tensile strength ($\chi = 10$MPa), asymptotic friction angle ($\tan\phi = 10°$) and fracture energies $G_f^I = 10^{-2}$MN/m and $G_f^{IIa} = 10^{-1}$MN/m. The specimen is subject to uniaxial compression loading along the horizontal direction

with boundary conditions as also shown in Fig.17 : increasing compressive displacements are prescribed to the right side of the specimen while the left side is allowed to move vertically.

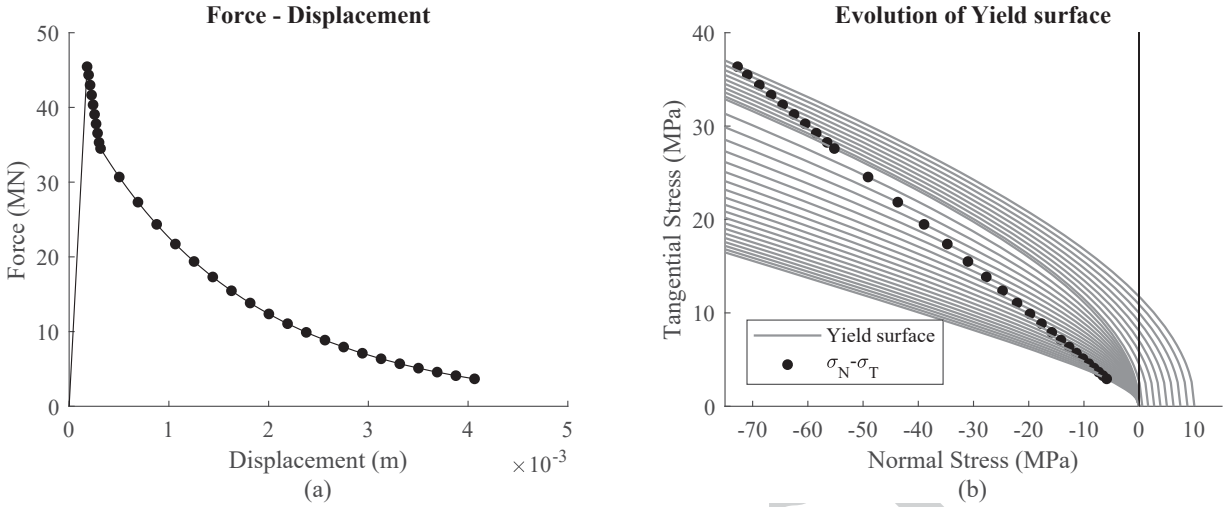

FIGURE 18 Results of exemple 3: (a) Resulting force-displacement diagram for whole specimen. (b) Evolution of normal and tangential stress on the discontinuity plane, and by yield surface evolution.

The results obtained are represented in Figures 18 and 19 . In Fig.18 a the resulting force-displacement curve for the whole specimen exhibits an elastic part, followed by a peak value and softening branch, corresponding to the sliding with friction and softening along the discontinuity. In Fig.18 b, the evolution of normal and shear stress on the discontinuity plane are represented together with the plastic surface at each stage of loading. It can be observed that the relation between normal and shear stress is (in this example) fixed by static condition along a straight line, while the hyperbolic surface is progressively degraded as the fracture process evolves.

Finally, Fig.19 represents the deformed shape of specimen at the end of the test, showing that the left part of specimen has moved upwards as the right part moved to the left, as required by discontinuity kinematics.

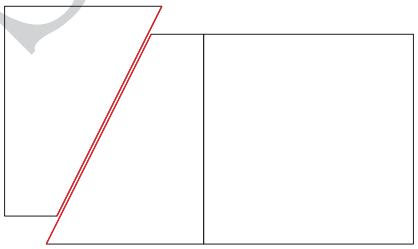

FIGURE 19 Magnified final deformation of specimen.

6 | CONCLUDING REMARKS

A particular version of XFEM is proposed in this paper, which is based on a double interpolation (or sub-interpolation) within each subdomain, and on the use of the "overhang" nodal displacements across the discontinuity (rather than the more usual jump variables themselves). The formulation turns out advantageous from various viewpoints. From the theoretical viewpoint, a direct relation may be established with the traditional formulation of the FEM with zero-thickness interface elements inserted along the same discontinuity line. In the paper, full equivalence is proven in the case of quadrangular elements crossed by a discontinuity in a "2-2" configuration. In other configurations (such as "1-3" quadrangular elements, or in the case of triangles), the equivalence is to a restricted version of the FEM+z formulation, in which the original kinematic variables would not be all independent. It is also noted that the element stiffness matrix and force vector has been developed on the basis of the Principle of Virtual Work, which, although a standard procedure in the FEM, that seems not reported in existing XFEM literature.

From the numerical viewpoint, the double-interpolation approach also seems to lead to favorable results w.r.t. formulations based on natural interpolation in the case of quadrangular elements when the discontinuity runs skew to the mesh. The reason for this and numerical example showing the improvement obtained have been included in Appendix D. Example 5.1 corroborates numerically that, in the case of triangles, sub-interpolation would be equivalent to the usual XFEM formulation using natural interpolation functions, something already argued from the theoretical viewpoint. This example also shows that, in general, quadrangular elements seem to perform much better than triangles for similar mesh densities, and also seem to be much less sensitive to high discontinuity (penalty) stiffness values, which in the case of triangles may easily lead to oscillations. The second example (tunnel cross-section) illustrates the numerical oscillations that may be observed when nodes lie too close to the discontinuity lines, and the effectivity of the strategy of moving those nodes onto the discontinuity line itself, provided of course that the resulting element configurations are properly identified and treated as special cases. This improvement is consistent with the fact that by doing this, the formulation becomes locally equivalent to FEM+z, maximizing the number of degrees of freedom to represent the discontinuity (not a restricted version). Finally, the third example illustrates the applicability of the formulation presented in combination with non-linear constitutive laws for the discontinuity.

ACKNOWLEDGMENTS

The work was partially supported by research grants BIA2016-76543-R from MEC (Madrid), which includes FEDER funds from the European Union, and 2017SGR-1153 from Generalitat de Catalunya (Barcelona). The first author would like to thank the MICINN (Madrid) for her FPI doctoral fellowship.

References

1. Mosler J., Meschke G.. Embedded crack vs. smeared crack models: a comparison of elementwise discontinuous crack path approaches with emphasis on mesh bias. *Computer Methods in Applied Mechanics and Engineering.* 2004;193(30-32):3351–3375.

2. Oliver J. A consistent characteristic length for smeared cracking models. *International Journal for Numerical Methods in Engineering.* 1989;28(2):461–474.

3. Weihe S, Kröplin B, De Borst R. Classification of smeared crack models based on material and structural properties. *International Journal of Solids and Structures.* 1998;35(12):1289–1308.

4. Gens A., Carol I., Alonso E.E.. An interface element formulation for the analysis of soil-reinforcement interaction. *Computers and Geotechnics.* 1989;7(1):133-151. Special Issue on Soil Reinforcement.

5. Carol Ignacio, Prat Pere C, López Carlos M. Normal/shear cracking model: application to discrete crack analysis. *Journal of engineering mechanics.* 1997;123(8):765–773.

6. Kaliakin V N, Li J. Insight into deficiencies associated with commonly used zero-thickness interface elements. *Computers and Geotechnics.* 1995;17(2):225–252.

7. Manzoli OL, Shing PB. Finite elements with embedded multiple cracks and non-uniform discontinuity modes. *Latin American Journal of Solids and Structures.* 2005;.

8. Linder Christian, Armero F. Finite elements with embedded strong discontinuities for the modeling of failure in solids. *International Journal for Numerical Methods in Engineering.* 2007;72(12):1391–1433.

9. Alfaiate J, Simone A, Sluys L J. Non-homogeneous displacement jumps in strong embedded discontinuities. *International Journal of Solids and Structures.* 2003;40(21):5799–5817.

10. Jirásek Milan. Comparative study on finite elements with embedded discontinuities. *Computer methods in applied mechanics and engineering.* 2000;188(1):307–330.

11. Belytschko T, Parimi C, Moës N, Sukumar N, Usui S. Structured extended finite element methods for solids defined by implicit surfaces. *International journal for numerical methods in engineering.* 2003;56(4):609–635.

12. Belytschko T, Gracie R. On XFEM applications to dislocations and interfaces. *International Journal of Plasticity.* 2007;23(10):1721–1738.

13. Fries Thomas-Peter, Belytschko Ted. The intrinsic XFEM: a method for arbitrary discontinuities without additional unknowns. *International journal for numerical methods in engineering.* 2006;68(13):1358–1385.

14. Fries Thomas-Peter, Belytschko Ted. The extended/generalized finite element method: an overview of the method and its applications. *International Journal for Numerical Methods in Engineering.* 2010;84(3):253–304.

15. Sukumar N., Chopp D.L., Moës N., Belytschko T.. Modeling holes and inclusions by level sets in the extended finite-element method. *Computer Methods in Applied Mechanics and Engineering.* 2001;190(46-47):6183–6200.

16. Mohammadi Soheil. *Extended finite element method: for fracture analysis of structures*. Blackwell Publishing Ltd; 2008.

17. Shibanuma Kazuki, Utsunomiya Tomoaki. Evaluation on reproduction of priori knowledge in XFEM. *Finite Elements in Analysis and Design.* 2011;47(4):424-433.

18. Pathak Himanshu, Singh Akhilendra, Singh Indra Vir. Fatigue crack growth simulations of 3-D problems using XFEM. *International Journal of Mechanical Sciences.* 2013;76:112-131.

19. Chen L, Rabczuk T, Bordas SP, Liu GR, Zeng KY, Kerfriden P. Extended finite element method with edge-based strain smoothing (ESM-XFEM) for linear elastic crack growth. *Computer Methods in Applied Mechanics and Engineering*. 2012;:250-265.

20. Shedbale AS, Singh IV, Mishra BK. Nonlinear Simulation of an Embedded Crack in the Presence of Holes and Inclusions by XFEM. *Procedia Engineering.* 2013;64:642-651. International Conference on Design and Manufacturing (IConDM2013).

21. Kumar Sachin, Singh IV, Mishra BK. Numerical Investigation of Stable Crack Growth in Ductile Materials Using XFEM. *Procedia Engineering.* 2013;64:652-660. International Conference on Design and Manufacturing (IConDM2013).

22. Jirásek Milan, Belytschko Ted. Computational Resolution of Strong Discontinuities. In: H.A. Mang F.G. Rammerstorfer, Eberhardsteiner J., eds. *Fifth World Congress on Computational Mechanics*, WCCM V Fifth World Congress on Computational Mechanics; 2002.

23. Moës Nicolas, Béchet Eric, Tourbier Matthieu. Imposing Dirichlet boundary conditions in the extended finite element method. *International Journal for Numerical Methods in Engineering.* 2006;67(12):1641–1669.

24. Sanders Jessica D., Dolbow John E., Laursen Tod A.. On methods for stabilizing constraints over enriched interface in elasticity. *International Journal for Numerical Methods in Engineering.* 2009;78(9):1009-1036.

25. Laborde Patrick, Pommier Julien, Renard Yves, Salaün Michel. High order extended finite element method for cracked domains. *International Journal for Numerical Methods in Engineering.* 2005;64(3):354–381.

26. Choi Young Joon, Hulsen Martien A., Meijer Han E.H.. Simulation of the flow of a viscoelastic fluid around a stationary cylinder using an extended finite element method. *Computers & Fluids.* 2012;57:183-194.

27. Zienkiewicz Olek C., Taylor. Robert L.. *The finite element method for solid and structural mechanics*. Butterworth-heinemann; 2005.

28. Kirsch E.G.. Die Theorie der Elastizität und die Bedürfnisse der Festigkeitslehre. *Zeitschrift des Vereines deutscher Ingenieure*. 1898;42:797-807.

How to cite this article: L. Crusat, I. Carol, and D. Garolera (2018), XFEM formulation with sub-interpolation, and equivalence to zero-thickness interface elements, *Int J Numer Anal Methods Geomech.*, *2018;XX*.

APPENDIX

A INTERPOLATION MATRIX $\bar{\mathbf{N}}$ FOR THE "2-2" AND "1-3" CONFIGURATIONS OF QUADRANGULAR ELEMENTS

In this appendix, the above shape function matrices will be specified for quadrangular elements. The same exercise for triangles is included in Apendix C.

In quadrangular elements, the vector of unknowns is:

$$\bar{\boldsymbol{u}}_e = \left(\boldsymbol{u}_{(1)}^T \; \boldsymbol{u}_{(2)}^T \; \boldsymbol{u}_{(3)}^T \; \boldsymbol{u}_{(4)}^T \;\middle|\; \boldsymbol{\delta}_{(1)}^T \; \boldsymbol{\delta}_{(2)}^T \; \boldsymbol{\delta}_{(3)}^T \; \boldsymbol{\delta}_{(4)}^T \right)^T \tag{A1}$$

For these elements it is possible to distinguish two basic configuration depending on the discontinuity position, which are denoted "2-2" or "1-3" (Fig. 5).

A.1 "2-2" configuration

The geometry of a quadrangular element with a "2-2" intersection is shown in Fig.5 a. Intersection points will be called α and β; α is located between nodes 1 and 2, and β between 4 and 3. The element domain is divided into three parts: The negative domain Ω^-, the positive domain Ω^+ and discontinuity itself (line α to β).

1. Negative subdomain:

   On the negative side, vector $\boldsymbol{u}_e^-$, and matrices $\hat{\mathbf{N}}^-$ and $\mathbf{T}^-$ have the following components:

$$\boldsymbol{u}_e^- = \left(\boldsymbol{u}_{(1)}^T \; \boldsymbol{u}_{(\alpha^-)}{}^T \; \boldsymbol{u}_{(\beta^-)}{}^T \; \boldsymbol{u}_{(4)}^T \right)^T \tag{A2}$$

$$\hat{\mathbf{N}}^- = \left[\begin{array}{cc|cc|cc|cc} \hat{N}_{(1)}^- & 0 & \hat{N}_{(\alpha)}^- & 0 & \hat{N}_{(\beta)}^- & 0 & \hat{N}_{(4)}^- & 0 \\ 0 & \hat{N}_{(1)}^- & 0 & \hat{N}_{(\alpha)}^- & 0 & \hat{N}_{(\beta)}^- & 0 & \hat{N}_{(4)}^- \end{array} \right] = \\ = \left[\hat{N}_{(1)}^- \mathbf{I} \middle| \; \hat{N}_{(\alpha)}^- \mathbf{I} \middle| \; \hat{N}_{(\beta)}^- \mathbf{I} \middle| \; \hat{N}_{(4)}^- \mathbf{I} \right] \tag{A3}$$

$$\mathbf{T}^- = \left[\begin{array}{ccccc|cccc} \mathbf{I} & \mathbf{0} & \mathbf{0} & \mathbf{0} & & \mathbf{0} & \mathbf{0} & \mathbf{0} & \mathbf{0} \\ N_{(1)}(\alpha)\mathbf{I} & \mathbf{0} & \mathbf{0} & \mathbf{0} & & \mathbf{0} & N_{(2)}(\alpha)\mathbf{I} & \mathbf{0} & \mathbf{0} \\ \mathbf{0} & \mathbf{0} & \mathbf{0} & N_{(4)}(\beta)\mathbf{I} & & \mathbf{0} & \mathbf{0} & N_{(3)}(\beta)\mathbf{I} & \mathbf{0} \\ \mathbf{0} & \mathbf{0} & \mathbf{0} & \mathbf{I} & & \mathbf{0} & \mathbf{0} & \mathbf{0} & \mathbf{0} \end{array} \right] \tag{A4}$$

   Therefore, the format of the resulting overall interpolation matrix $\bar{\mathbf{N}}^-$ is:

$$\bar{\mathbf{N}}^- = \hat{\mathbf{N}}^- \mathbf{T}^- = \left[\bar{\mathbf{N}}_u^- \middle| \; \bar{\mathbf{N}}_\delta^- \right] \tag{A5}$$

   where

$$\bar{\mathbf{N}}_u^- = \left[\left(\hat{N}_{(1)}^- + \hat{N}_{(\alpha)}^- N_{(1)}(\alpha) \right) \mathbf{I}\ \mathbf{0}\ \mathbf{0}\ \left(\hat{N}_{(\beta)}^- N_{(4)}(\beta) + \hat{N}_{(4)}^- \right) \mathbf{I} \right] \tag{A6}$$

$$\bar{\mathbf{N}}_\delta^- = \left[\mathbf{0}\ \left(\hat{N}_{(\alpha)}^- N_{(2)}(\alpha) \right) \mathbf{I}\ \left(\hat{N}_{(\beta)}^- N_{(3)}(\beta) \right) \mathbf{I}\ \mathbf{0} \right] \tag{A7}$$

2. *P*ositive subdomain:

On the positive side, vector $\boldsymbol{u}_e^{\,+}$, and matrices $\hat{\mathbf{N}}^+$ and $\mathbf{T}^+$ have the following components:

$$\boldsymbol{u}_e^{\,+} = \left(\boldsymbol{u}_{(\alpha^+)}^T\ \boldsymbol{u}_{(2)}^T\ \boldsymbol{u}_{(3)}^T\ \boldsymbol{u}_{(\beta^+)}^T \right)^T \tag{A8}$$

$$\hat{\mathbf{N}}^+ = \left[\begin{array}{cc|cc|cc|cc} \hat{N}_{(\alpha)}^+ & 0 & \hat{N}_{(2)}^+ & 0 & \hat{N}_{(3)}^+ & 0 & \hat{N}_{(\beta)}^+ & 0 \\ 0 & \hat{N}_{(\alpha)}^+ & 0 & \hat{N}_{(2)}^+ & 0 & \hat{N}_{(3)}^+ & 0 & \hat{N}_{(\beta)}^+ \end{array} \right] = \\ = \left[\hat{N}_{(\alpha)}^+ \mathbf{I} \middle|\ \hat{N}_{(2)}^+ \mathbf{I} \middle|\ \hat{N}_{(3)}^+ \mathbf{I} \middle|\ \hat{N}_{(\beta)}^+ \mathbf{I} \right] \tag{A9}$$

$$\mathbf{T}^+ = \left[\begin{array}{cccc|cccc} \mathbf{0} & N_{(2)}(\alpha)\mathbf{I} & \mathbf{0} & \mathbf{0} & N_{(1)}(\alpha)\mathbf{I} & \mathbf{0} & \mathbf{0} & \mathbf{0} \\ \mathbf{0} & \mathbf{I} & \mathbf{0} & \mathbf{0} & \mathbf{0} & \mathbf{0} & \mathbf{0} & \mathbf{0} \\ \mathbf{0} & \mathbf{0} & \mathbf{I} & \mathbf{0} & \mathbf{0} & \mathbf{0} & \mathbf{0} & \mathbf{0} \\ \mathbf{0} & \mathbf{0} & N_{(3)}(\beta)\mathbf{I} & \mathbf{0} & \mathbf{0} & \mathbf{0} & \mathbf{0} & N_{(4)}(\beta)\mathbf{I} \end{array} \right] \tag{A10}$$

Therefore, the format of the resulting overall interpolation matrix $\bar{\mathbf{N}}^+$ is:

$$\bar{\mathbf{N}}^+ = \hat{\mathbf{N}}^+ \mathbf{T}^+ = \left[\bar{\mathbf{N}}_u^+ \middle|\ \bar{\mathbf{N}}_\delta^+ \right] \tag{A11}$$

where

$$\bar{\mathbf{N}}_u^+ = \left[\mathbf{0}\ \left(\hat{N}_{(\alpha)}^+ N_{(2)}(\alpha) + \hat{N}_{(2)}^+ \right) \mathbf{I}\ \left(\hat{N}_{(3)}^+ + \hat{N}_{(\beta)}^+ N_{(3)}(\beta) \right) \mathbf{I}\ \mathbf{0} \right] \tag{A12}$$

$$\bar{\mathbf{N}}_\delta^+ = \left[\left(\hat{N}_{(\alpha)}^+ N_{(1)}(\alpha) \right) \mathbf{I}\ \mathbf{0}\ \mathbf{0}\ \left(\hat{N}_{(\beta)}^+ N_{(4)}(\beta) \right) \mathbf{I} \right] \tag{A13}$$

3. *D*iscontinuity:

Along the discontinuity itself, the key kinematic variable is the displacement jump, which is equal to the difference between the displacement on each side of the discontinuity.

$$\boldsymbol{a}(\boldsymbol{x}) = \boldsymbol{u}\left(\boldsymbol{x}_{(J)}^+ \right) - \boldsymbol{u}\left(\boldsymbol{x}_{(J)}^- \right) = \\ = \left[\bar{\mathbf{N}}_u^+ - \bar{\mathbf{N}}_u^- \middle|\ \bar{\mathbf{N}}_\delta^+ - \bar{\mathbf{N}}_\delta^- \right] \begin{pmatrix} \boldsymbol{u}_e \\ \boldsymbol{\delta}_e \end{pmatrix} = \\ = \bar{\mathbf{N}}^J \bar{\boldsymbol{u}}_e \tag{A14}$$

Note that, along the discontinuity $\boldsymbol{x}^J \in \overline{\alpha\beta}$, $\hat{N}_{(\lambda)}^+(\boldsymbol{x}^J) = \hat{N}_{(\lambda)}^-(\boldsymbol{x}^J) = \hat{N}_{(\lambda)}(\boldsymbol{x}^J)$ for $\lambda = \alpha, \beta$. And $\hat{N}_{(1)}^-(\boldsymbol{x}^J) = \hat{N}_{(4)}^-(\boldsymbol{x}^J) = \hat{N}_{(2)}^+(\boldsymbol{x}^J) = \hat{N}_{(3)}^+(\boldsymbol{x}^J) = 0$, which leads to:

$$\bar{\mathbf{N}}_u^J = \bar{\mathbf{N}}_u^+ - \bar{\mathbf{N}}_u^- = \\ = \left[-\hat{N}_{(\alpha)} N_{(1)}(\alpha)\mathbf{I} \middle|\ \hat{N}_{(\alpha)} N_{(2)}(\alpha)\mathbf{I} \middle|\ \hat{N}_{(\beta)} N_{(3)}(\beta)\mathbf{I} \middle|\ -\hat{N}_{(\beta)} N_{(4)}(\beta)\mathbf{I} \right] \tag{A15}$$

$$\bar{\mathbf{N}}_\delta^J = \bar{\mathbf{N}}_\delta^+ - \bar{\mathbf{N}}_\delta^- = \\ = \left[\hat{N}_{(\alpha)} N_{(1)}(\alpha)\mathbf{I} \middle|\ -\hat{N}_{(\alpha)} N_{(2)}(\alpha)\mathbf{I} \middle|\ -\hat{N}_{(\beta)} N_{(3)}(\beta)\mathbf{I} \middle|\ \hat{N}_{(\beta)} N_{(4)}(\beta)\mathbf{I} \right] \tag{A16}$$

The above expressions may be also rewritten in the following way

$$\bar{\mathbf{N}}^{J} = \hat{\mathbf{N}}^{J}\mathbf{T}^{J} \tag{A17}$$

where

$$\hat{\mathbf{N}}^{J} = \left[-\hat{N}_{(\beta)}\mathbf{I} \middle| -\hat{N}_{(\alpha)}\mathbf{I} \middle| \hat{N}_{(\beta)}\mathbf{I} \middle| \hat{N}_{(\alpha)}\mathbf{I} \right] \tag{A18}$$

$$\mathbf{T}^{J} = \left[\begin{array}{cccc|cccc} \mathbf{0} & \mathbf{0} & \mathbf{0} & N_{(4)}(\beta)\mathbf{I} & \mathbf{0} & \mathbf{0} & N_{(3)}(\beta)\mathbf{I} & \mathbf{0} \\ N_{(1)}(\alpha)\mathbf{I} & \mathbf{0} & \mathbf{0} & \mathbf{0} & \mathbf{0} & N_{(2)}(\alpha)\mathbf{I} & \mathbf{0} & \mathbf{0} \\ \mathbf{0} & \mathbf{0} & N_{(3)}(\beta)\mathbf{I} & \mathbf{0} & \mathbf{0} & \mathbf{0} & \mathbf{0} & N_{(4)}(\beta)\mathbf{I} \\ \mathbf{0} & N_{(2)}(\alpha)\mathbf{I} & \mathbf{0} & \mathbf{0} & N_{(1)}(\alpha)\mathbf{I} & \mathbf{0} & \mathbf{0} & \mathbf{0} \end{array}\right] \tag{A19}$$

A.2 "1-3" configurations

In this configuration, the discontinuity divides the quadrangular element into a triangular ("negative") part with only one node, and a pentagonal ("positive") part containing three nodes. Since, eventually, an integral has to be performed over each element subdomain, the pentagonal part is further subdivided into three triangular subdomains Ω^{+1},Ω^{+2} and Ω^{+3}, while the negative part is maintained as a single triangular subdomain Ω^{-} (Fig.5 b).

1. *N*egative subdomain:

   In the negative (triangular) subdomain (Fig. 5 b), vector $\boldsymbol{u}_e^{-}$, and matrices $\hat{\mathbf{N}}^{-}$ and $\mathbf{T}^{-}$ have the following structure:

$$\boldsymbol{u}_e^{-} = \left(\boldsymbol{u}_{(\alpha^-)}{}^{T} \; \boldsymbol{u}_{(\beta^-)}{}^{T} \; \boldsymbol{u}_{(4)}^{T} \right)^{T} \tag{A20}$$

$$\hat{\mathbf{N}}^{-} = \left[\begin{array}{cc|cc|cc} \hat{N}_{(\alpha)} & 0 & \hat{N}_{(\beta)} & 0 & \hat{N}_{(4)} & 0 \\ 0 & \hat{N}_{(\alpha)} & 0 & \hat{N}_{(\beta)} & 0 & \hat{N}_{(4)} \end{array}\right] = \\ = \left[\hat{N}_{(\alpha)}\mathbf{I} \middle| \hat{N}_{(\beta)}\mathbf{I} \middle| \hat{N}_{(4)}\mathbf{I} \right] \tag{A21}$$

$$\mathbf{T}^{-} = \left[\begin{array}{ccc|cccc} \mathbf{0} & \mathbf{0} & \mathbf{0} & N_{(4)}(\alpha)\mathbf{I} & N_{(1)}(\alpha)\mathbf{I} & \mathbf{0} & \mathbf{0} & \mathbf{0} \\ \mathbf{0} & \mathbf{0} & \mathbf{0} & N_{(4)}(\beta)\mathbf{I} & \mathbf{0} & \mathbf{0} & N_{(3)}(\beta)\mathbf{I} & \mathbf{0} \\ \mathbf{0} & \mathbf{0} & \mathbf{0} & \mathbf{I} & \mathbf{0} & \mathbf{0} & \mathbf{0} & \mathbf{0} \end{array}\right] \tag{A22}$$

   Therefore, the resulting overall interpolation matrix $\bar{\mathbf{N}}^{-}$ is:

$$\bar{\mathbf{N}}^{-} = \left[\bar{\mathbf{N}}_u^{-} \middle| \bar{\mathbf{N}}_\delta^{-} \right] \tag{A23}$$

   where

$$\bar{\mathbf{N}}_u^{-} = \left[\mathbf{0} \middle| \mathbf{0} \middle| \mathbf{0} \middle| \left(\hat{N}_{(\alpha)} N_{(4)}(\alpha) + \hat{N}_{(\beta)} N_{(4)}(\beta) + \hat{N}_{(4)} \right) \mathbf{I} \right] \tag{A24}$$

$$\bar{\mathbf{N}}_\delta^{-} = \left[\hat{N}_{(\alpha)} N_{(1)}(\alpha)\mathbf{I} \middle| \mathbf{0} \middle| \hat{N}_{(\beta)} N_{(3)}(\beta)\mathbf{I} \middle| \mathbf{0} \right] \tag{A25}$$

2. *P*ositive subdomain:

   As already mentioned, the pentagonal positive part of the element is in turn subdivided into three triangle subdomains denoted as Ω^{+1}, Ω^{+2} and Ω^{+3}, see Fig.5 b.

   Subdomain Ω^{+1} is formed by nodes 1, 2 and α. Consequently, vector $\boldsymbol{u}_e^{+1}$, and matrices $\hat{\mathbf{N}}^{+1}$ and $\mathbf{T}^{+1}$ have the following components:

$$\boldsymbol{u}_e^{+1} = \left(\boldsymbol{u}_{(1)}^{T} \; \boldsymbol{u}_{(2)}^{T} \; \boldsymbol{u}_{(\alpha^+)}{}^{T} \right)^{T} \tag{A26}$$

$$\hat{\mathbf{N}}^{+1} = \left[\begin{array}{cc|cc|cc} \hat{N}_{(1)} & 0 & \hat{N}_{(2)} & 0 & \hat{N}_{(\alpha)} & 0 \\ 0 & \hat{N}_{(1)} & 0 & \hat{N}_{(2)} & 0 & \hat{N}_{(\alpha)} \end{array}\right] = \left[\begin{array}{c|c|c} \hat{N}_{(1)}\mathbf{I} & \hat{N}_{(2)}\mathbf{I} & \hat{N}_{(\alpha)}\mathbf{I} \end{array}\right] \tag{A27}$$

$$\mathbf{T}^{+1} = \left[\begin{array}{cccc|cccc} \mathbf{I} & \mathbf{0} & \mathbf{0} & \mathbf{0} & \mathbf{0} & \mathbf{0} & \mathbf{0} & \mathbf{0} \\ \mathbf{0} & \mathbf{I} & \mathbf{0} & \mathbf{0} & \mathbf{0} & \mathbf{0} & \mathbf{0} & \mathbf{0} \\ N_{(1)}(\alpha)\mathbf{I} & \mathbf{0} & \mathbf{0} & \mathbf{0} & \mathbf{0} & \mathbf{0} & \mathbf{0} & N_{(4)}(\alpha)\mathbf{I} \end{array}\right] \tag{A28}$$

Therefore, the resulting overall interpolation matrix $\bar{\mathbf{N}}^{+1}$ is:

$$\bar{\mathbf{N}}^{+1} = \left[\begin{array}{c|c} \bar{\mathbf{N}}_u^{+1} & \bar{\mathbf{N}}_\delta^{+1} \end{array}\right] \tag{A29}$$

where

$$\bar{\mathbf{N}}_u^{+1} = \left[\begin{array}{c|c|c|c} \left(\hat{N}_{(1)} + \hat{N}_{(\alpha)}N_{(1)}(\alpha)\right)\mathbf{I} & \hat{N}_{(2)}\mathbf{I} & \mathbf{0} & \mathbf{0} \end{array}\right] \tag{A30}$$

$$\bar{\mathbf{N}}_\delta^{+1} = \left[\begin{array}{c|c|c|c} \mathbf{0} & \mathbf{0} & \mathbf{0} & \hat{N}_{(\alpha)}N_{(4)}(\alpha)\mathbf{I} \end{array}\right] \tag{A31}$$

Subdomain Ω^{+2} is formed by nodes α^+, 2 and β^+. Vector $\boldsymbol{u}_e{}^{+2}$, matrix $\hat{\mathbf{N}}^{+2}$ and $\mathbf{T}^{+2}$ have the following components:

$$\boldsymbol{u}_e{}^{+2} = \left(\boldsymbol{u}_{(\alpha^+)}{}^T \; \boldsymbol{u}_{(2)}^T \; \boldsymbol{u}_{(\alpha^+)}{}^T\right)^T \tag{A32}$$

$$\hat{\mathbf{N}}^{+2} = \left[\begin{array}{cc|cc|cc} \hat{N}_{(\alpha)} & 0 & \hat{N}_{(2)} & 0 & \hat{N}_{(\beta)} & 0 \\ 0 & \hat{N}_{(\alpha)} & 0 & \hat{N}_{(2)} & 0 & \hat{N}_{(\beta)} \end{array}\right] = \left[\begin{array}{c|c|c} \hat{N}_{(\alpha)}\mathbf{I} & \hat{N}_{(2)}\mathbf{I} & \hat{N}_{(\beta)}\mathbf{I} \end{array}\right] \tag{A33}$$

$$\mathbf{T}^{+2} = \left[\begin{array}{cccc|cccc} N_{(1)}(\alpha)\mathbf{I} & 0 & \mathbf{0} & \mathbf{0} & \mathbf{0} & \mathbf{0} & \mathbf{0} & N_{(4)}(\alpha)\mathbf{I} \\ \mathbf{0} & \mathbf{I} & \mathbf{0} & \mathbf{0} & \mathbf{0} & \mathbf{0} & \mathbf{0} & 0 \\ \mathbf{0} & \mathbf{0} & N_{(3)}(\beta)\mathbf{I} & \mathbf{0} & \mathbf{0} & \mathbf{0} & \mathbf{0} & N_{(4)}(\beta)\mathbf{I} \end{array}\right] \tag{A34}$$

Therefore, the resulting overall interpolation matrix $\bar{\mathbf{N}}^{+2}$ is:

$$\bar{\mathbf{N}}^{+2} = \left[\begin{array}{c|c} \bar{\mathbf{N}}_u^{+2} & \bar{\mathbf{N}}_\delta^{+2} \end{array}\right] \tag{A35}$$

where

$$\bar{\mathbf{N}}_u^{+2} = \left[\begin{array}{c|c|c|c} \hat{N}_{(\alpha)}N_{(1)}(\alpha)\mathbf{I} & \hat{N}_{(2)}\mathbf{I} & \hat{N}_{(\beta)}N_{(3)}(\beta)\mathbf{I} & \mathbf{0} \end{array}\right] \tag{A36}$$

$$\bar{\mathbf{N}}_\delta^{+2} = \left[\begin{array}{c|c|c|c} \mathbf{0} & \mathbf{0} & \mathbf{0} & \left(\hat{N}_{(\alpha)}N_{(4)}(\alpha) + \hat{N}_{(\beta)}N_{(4)}(\beta)\right)\mathbf{I} \end{array}\right] \tag{A37}$$

Subdomain $\Omega^{(+3)}$ is formed by nodes 2, 3 and β. So integration is done with shape functions of this subdomain, vector $\boldsymbol{u}_e{}^{+3}$, and matrices $\hat{\mathbf{N}}^{+3}$ and $\mathbf{T}^{+3}$ have the following components:

$$\boldsymbol{u}_e{}^{+3} = \left(\boldsymbol{u}_{(2)}^T \; \boldsymbol{u}_{(3)}^T \; \boldsymbol{u}_{(\beta^+)}{}^T\right)^T \tag{A38}$$

$$\hat{\mathbf{N}}^{+3} = \left[\begin{array}{cc|cc|cc} \hat{N}_{(2)} & 0 & \hat{N}_{(3)} & 0 & \hat{N}_{(\beta)} & 0 \\ 0 & \hat{N}_{(2)} & 0 & \hat{N}_{(3)} & 0 & \hat{N}_{(\beta)} \end{array}\right] = \left[\begin{array}{c|c|c} \hat{N}_{(2)}\mathbf{I} & \hat{N}_{(3)}\mathbf{I} & \hat{N}_{(\beta)}\mathbf{I} \end{array}\right] \tag{A39}$$

$$\mathbf{T}^{+3} = \left[\begin{array}{cccc|cccc} \mathbf{0}\,\mathbf{I} & \mathbf{0} & \mathbf{0} & & \mathbf{0}\,\mathbf{0}\,\mathbf{0} & \mathbf{0} & \\ \mathbf{0}\,\mathbf{0} & \mathbf{I} & \mathbf{0} & & \mathbf{0}\,\mathbf{0}\,\mathbf{0} & \mathbf{0} & \\ \mathbf{0}\,\mathbf{0} & N_{(3)}(\beta)\,\mathbf{I} & \mathbf{0} & & \mathbf{0}\,\mathbf{0}\,\mathbf{0} & N_{(4)}(\beta)\,\mathbf{I} & \end{array}\right] \tag{A40}$$

Therefore, the resulting overall interpolation matrix $\bar{\mathbf{N}}^{+3}$ is:

$$\bar{\mathbf{N}}^{+3} = \left[\begin{array}{c|c} \bar{\mathbf{N}}_u^{+3} & \bar{\mathbf{N}}_\delta^{+3} \end{array}\right] \tag{A41}$$

where

$$\bar{\mathbf{N}}_u^{+3} = \left[\begin{array}{c|c|c|c} \mathbf{0} & \hat{N}_{(2)}\mathbf{I} & \left(\hat{N}_{(3)} + \hat{N}_{(\beta)}N_{(3)}(\beta)\right)\mathbf{I} & \mathbf{0} \end{array}\right] \tag{A42}$$

$$\bar{\mathbf{N}}_\delta^{+3} = \left[\begin{array}{ccc} \mathbf{0} & \mathbf{0} & \mathbf{0} \end{array}\right. \left|\begin{array}{c} \hat{N}_{(\beta)}N_{(4)}(\beta)\,\mathbf{I} \end{array}\right] \tag{A43}$$

3. *D*iscontinuity:

Along the discontinuity itself, the key kinematic variable is the displacement jump, which is equal to the difference between the displacement on each side of the discontinuity.

$$\begin{aligned} \boldsymbol{a}(\boldsymbol{x}) &= \boldsymbol{u}\left(\boldsymbol{x}^{J^{+2}}\right) - \boldsymbol{u}\left(\boldsymbol{x}^{J^{-}}\right) = \\ &= \left[\begin{array}{c|c} \bar{\mathbf{N}}_u^{+2} - \bar{\mathbf{N}}_u^{-} & \bar{\mathbf{N}}_\delta^{+2} - \bar{\mathbf{N}}_\delta^{-} \end{array}\right] \begin{pmatrix} \boldsymbol{u}_e \\ \boldsymbol{\delta}_e \end{pmatrix} = \bar{\mathbf{N}}^J \bar{\boldsymbol{u}}_e \end{aligned} \tag{A44}$$

Note that, along the discontinuity $\boldsymbol{x}^J \in \overline{\alpha\beta}$, $\hat{N}_{(\lambda)}^{+2}\left(\boldsymbol{x}^J\right) = \hat{N}_{(\lambda)}^{-}\left(\boldsymbol{x}^J\right) = \hat{\mathbf{N}}_{(\lambda)}\left(\boldsymbol{x}^J\right)$ for $\lambda = \alpha, \beta$, and $\hat{N}_{(4)}^{-}\left(\boldsymbol{x}^J\right) = \hat{N}_{(1)}^{+2}\left(\boldsymbol{x}^J\right) = \hat{N}_{(2)}^{+2}\left(\boldsymbol{x}^J\right) = \hat{N}_{(3)}^{+2}\left(\boldsymbol{x}^J\right) = 0$, which leads to:

$$\begin{aligned} \bar{\mathbf{N}}_u^J &= \bar{\mathbf{N}}_u^{+2} - \bar{\mathbf{N}}_u^{-} = \\ &= \left[\begin{array}{c|c|c|c} \hat{N}_{(\alpha)}N_{(1)}(\alpha)\,\mathbf{I} & \mathbf{0} & \hat{N}_{(\beta)}N_{(3)}(\beta)\,\mathbf{I} & -\left(\hat{N}_{(\alpha)}N_{(4)}(\alpha) + \hat{N}_{(\beta)}N_{(4)}(\beta)\right)\mathbf{I} \end{array}\right] \end{aligned} \tag{A45}$$

$$\begin{aligned} \bar{\mathbf{N}}_\delta^J &= \bar{\mathbf{N}}_\delta^{+2} - \bar{\mathbf{N}}_\delta^{-} = \\ &= \left[\begin{array}{c|c|c|c} -\hat{N}_{(\alpha)}N_{(1)}(\alpha)\,\mathbf{I} & \mathbf{0} & -\hat{N}_{(\beta)}N_{(3)}(\beta)\,\mathbf{I} & \left(\hat{N}_{(\alpha)}N_{(4)}(\alpha) + \hat{N}_{(\beta)}N_{(4)}(\beta)\right)\mathbf{I} \end{array}\right] \end{aligned} \tag{A46}$$

The above expressions may be also rewritten in the following way

$$\bar{\mathbf{N}}^J = \hat{\mathbf{N}}^J \mathbf{T}^J \tag{A47}$$

where

$$\hat{\mathbf{N}}^J = \left[\begin{array}{c|c|c|c} -\hat{N}_{(\beta)}\mathbf{I} & -\hat{N}_{(\alpha)}\mathbf{I} & \hat{N}_{(\beta)}\mathbf{I} & \hat{N}_{(\alpha)}\mathbf{I} \end{array}\right] \tag{A48}$$

$$\mathbf{T}^J = \left[\begin{array}{cccc|cccc} \mathbf{0} & \mathbf{0} & \mathbf{0} & N_{(4)}(\beta)\,\mathbf{I} & \mathbf{0} & \mathbf{0}\,N_{(3)}(\beta)\,\mathbf{I} & \mathbf{0} & \\ \mathbf{0} & \mathbf{0} & \mathbf{0} & N_{(4)}(\alpha)\,\mathbf{I} & N_{(1)}(\alpha)\,\mathbf{I} & \mathbf{0} & \mathbf{0} & \\ \mathbf{0} & \mathbf{0}\,N_{(3)}(\beta)\,\mathbf{I} & \mathbf{0} & & \mathbf{0} & \mathbf{0} & \mathbf{0} & N_{(4)}(\beta)\,\mathbf{I} \\ N_{(1)}(\alpha)\,\mathbf{I} & \mathbf{0} & \mathbf{0} & \mathbf{0} & \mathbf{0} & \mathbf{0} & \mathbf{0} & N_{(4)}(\alpha)\,\mathbf{I} \end{array}\right] \tag{A49}$$

B INTERPOLATION MATRIX $\bar{\mathbf{N}}$ FOR SPECIAL CONFIGURATIONS OF QUADRANGULAR ELEMENTS

The special configurations of a discontinuity crossing a quadrangular element are represented in Fig. B1 .

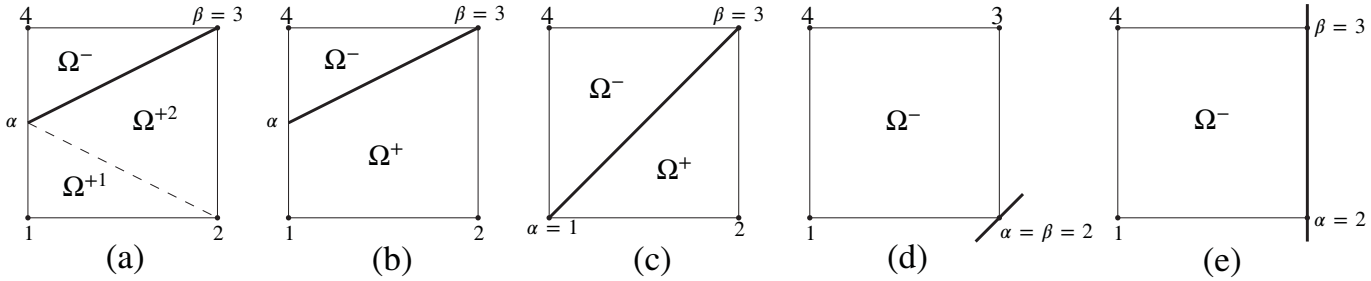

FIGURE B1 Special configurations for quadrangular elements (a) discontinuity coinciding with a node and crossing an edge (positive subdomain is discretized in two triangles). (b) discontinuity coinciding with a node and crossing an edge (positive subdomain is discretized in one quadrangle). (c) discontinuity coinciding with two node crossing diagonally the element. (d) discontinuity coinciding with only one node. (e) discontinuity coinciding with an edge.

B.1 Quadrangular element with special configuration for a discontinuity coinciding with a node and crossing an edge, and positive part subdivided into two triangular subdomains (Fig.B1 a)

Matrices $\hat{\mathbf{N}}^{-}$ and $\mathbf{T}^{-}$ for the triangular negative subdomain $\left(\Omega^{-}\right)$:

$$\hat{\mathbf{N}}^{-} = \left[\hat{N}^{-}_{(\alpha)}\mathbf{I} \middle| \hat{N}^{-}_{(3)}\mathbf{I} \middle| \hat{N}^{-}_{(4)}\mathbf{I} \right] \tag{B50}$$

$$\mathbf{T}^{-} = \left[\begin{array}{ccc|c|ccc} \mathbf{0} & \mathbf{0} & \mathbf{0} & N_{(4)}(\alpha)\mathbf{I} & N_{(1)}(\alpha)\mathbf{I} & \mathbf{0} & \mathbf{0} & \mathbf{0} \\ \mathbf{0} & \mathbf{0} & \mathbf{0} & \mathbf{0} & \mathbf{0} & \mathbf{0} & \mathbf{I} & \mathbf{0} \\ \mathbf{0} & \mathbf{0} & \mathbf{0} & \mathbf{I} & \mathbf{0} & \mathbf{0} & \mathbf{0} & \mathbf{0} \end{array}\right] \tag{B51}$$

Matrices $\hat{\mathbf{N}}^{+1}, \mathbf{T}^{+1}$ and $\hat{\mathbf{N}}^{+2}, \mathbf{T}^{+2}$ for the positive side divided into triangular subdomains $\left(\Omega^{+1}\right)$ and $\left(\Omega^{+2}\right)$:

$$\hat{\mathbf{N}}^{+1} = \left[\hat{N}^{+1}_{(1)}\mathbf{I} \middle| \hat{N}^{+1}_{(2)}\mathbf{I} \middle| \hat{N}^{+1}_{(\alpha)}\mathbf{I} \right] \tag{B52}$$

$$\mathbf{T}^{+1} = \left[\begin{array}{ccc|c|ccc} \mathbf{I} & \mathbf{0} & \mathbf{0} & \mathbf{0} & \mathbf{0} & \mathbf{0} & \mathbf{0} & \mathbf{0} \\ \mathbf{0} & \mathbf{I} & \mathbf{0} & \mathbf{0} & \mathbf{0} & \mathbf{0} & \mathbf{0} & \mathbf{0} \\ N_{(1)}(\alpha)\mathbf{I} & \mathbf{0} & \mathbf{0} & \mathbf{0} & \mathbf{0} & \mathbf{0} & \mathbf{0} & N_{(4)}(\alpha)\mathbf{I} \end{array}\right] \tag{B53}$$

$$\hat{\mathbf{N}}^{+2} = \left[\hat{N}^{+2}_{(\alpha)}\mathbf{I} \middle| \hat{N}^{+2}_{(2)}\mathbf{I} \middle| \hat{N}^{+2}_{(3)}\mathbf{I} \right] \tag{B54}$$

$$\mathbf{T}^{+2} = \left[\begin{array}{ccc|c|ccc} N_{(1)}(\alpha)\mathbf{I} & \mathbf{0} & \mathbf{0} & \mathbf{0} & \mathbf{0} & \mathbf{0} & \mathbf{0} & N_{(4)}(\alpha)\mathbf{I} \\ \mathbf{0} & \mathbf{I} & \mathbf{0} & \mathbf{0} & \mathbf{0} & \mathbf{0} & \mathbf{0} & \mathbf{0} \\ \mathbf{0} & \mathbf{0} & \mathbf{I} & \mathbf{0} & \mathbf{0} & \mathbf{0} & \mathbf{0} & \mathbf{0} \end{array}\right] \tag{B55}$$

Matrices $\hat{\mathbf{N}}^{J}$ and $\mathbf{T}^{J}$ on the discontinuity:

$$\hat{\mathbf{N}}^{J} = \left[-\hat{N}_{(3)}\mathbf{I} \middle| -\hat{N}_{(\alpha)}\mathbf{I} \middle| \hat{N}_{(3)}\mathbf{I} \middle| \hat{N}_{(\alpha)}\mathbf{I} \right] \tag{B56}$$

$$\mathbf{T}^{J} = \left[\begin{array}{ccc|c|ccc} \mathbf{0} & \mathbf{0} & \mathbf{0} & \mathbf{0} & \mathbf{0} & \mathbf{0} & \mathbf{I} & \mathbf{0} \\ \mathbf{0} & \mathbf{0} & \mathbf{0} & N_{(4)}(\alpha)\mathbf{I} & \mathbf{N}_{(1)}(\boldsymbol{\alpha})\mathbf{I} & \mathbf{0} & \mathbf{0} & \mathbf{0} \\ \mathbf{0} & \mathbf{0} & \mathbf{I} & \mathbf{0} & \mathbf{0} & \mathbf{0} & \mathbf{0} & \mathbf{0} \\ N_{(1)}(\alpha)\mathbf{I} & \mathbf{0} & \mathbf{0} & \mathbf{0} & \mathbf{0} & \mathbf{0} & \mathbf{0} & N_{(4)}(\alpha)\mathbf{I} \end{array}\right] \tag{B57}$$

B.2 Quadrangular element with special configuration for a discontinuity coinciding with a node and crossing an edge, and positive part taken as a single quadrangular subdomain (Fig.B1 b)

Matrices $\hat{\mathbf{N}}^{-}$ and $\mathbf{T}^{-}$ for the triangular negative subdomain are the same as (B50), (B51).

Matrices $\hat{\mathbf{N}}^{+}$ and $\mathbf{T}^{+}$ for the quadrangular positive subdomain:

$$\hat{\mathbf{N}}^{+} = \left[\hat{N}^{+}_{(1)}\mathbf{I} \middle| \hat{N}^{+}_{(2)}\mathbf{I} \middle| \hat{N}^{+}_{(3)}\mathbf{I} \middle| \hat{N}^{+}_{(\alpha)}\mathbf{I} \right] \tag{B58}$$

$$\mathbf{T}^{+} = \left[\begin{array}{cccc|ccc|c} \mathbf{I} & \mathbf{0}\,\mathbf{0}\,\mathbf{0} & \mathbf{0}\,\mathbf{0}\,\mathbf{0} & \mathbf{0} \\ \mathbf{0} & \mathbf{I}\,\mathbf{0}\,\mathbf{0} & \mathbf{0}\,\mathbf{0}\,\mathbf{0} & \mathbf{0} \\ \mathbf{0} & \mathbf{0}\,\mathbf{I}\,\mathbf{0} & \mathbf{0}\,\mathbf{0}\,\mathbf{0} & \mathbf{0} \\ N_{(1)}(\alpha)\mathbf{I} & \mathbf{0}\,\mathbf{0}\,\mathbf{0} & \mathbf{0}\,\mathbf{0}\,\mathbf{0} & N_{(4)}(\alpha)\mathbf{I} \end{array}\right] \tag{B59}$$

Matrices $\hat{\mathbf{N}}^{J}$ and $\mathbf{T}^{J}$ on the discontinuity are the same as (B56), (B57).

B.3 Quadrangular element with special configuration for a discontinuity coinciding with two nodes crossing diagonally the element (Fig.B1 c)

Matrices $\hat{\mathbf{N}}^{-}$ and $\mathbf{T}^{-}$ for the triangular negative subdomain:

$$\hat{\mathbf{N}}^{-} = \left[\hat{N}^{-}_{(1)}\mathbf{I} \middle| \hat{N}^{-}_{(3)}\mathbf{I} \middle| \hat{N}^{-}_{(4)}\mathbf{I} \right] \tag{B60}$$

$$\mathbf{T}^{-} = \left[\begin{array}{ccccccc} \mathbf{0}\,\mathbf{0}\,\mathbf{0}\,\mathbf{0} & \mathbf{I}\,\mathbf{0}\,\mathbf{0}\,\mathbf{0} \\ \mathbf{0}\,\mathbf{0}\,\mathbf{0}\,\mathbf{0} & \mathbf{0}\,\mathbf{0}\,\mathbf{I}\,\mathbf{0} \\ \mathbf{0}\,\mathbf{0}\,\mathbf{0}\,\mathbf{I} & \mathbf{0}\,\mathbf{0}\,\mathbf{0}\,\mathbf{0} \end{array}\right] \tag{B61}$$

Matrices $\hat{\mathbf{N}}^{+}$ and $\mathbf{T}^{+}$ for the triangular positive subdomain:

$$\hat{\mathbf{N}}^{+} = \left[\hat{N}^{+}_{(1)}\mathbf{I} \middle| \hat{N}^{+}_{(2)}\mathbf{I} \middle| \hat{N}^{+}_{(3)}\mathbf{I} \right] \tag{B62}$$

$$\mathbf{T}^{+} = \left[\begin{array}{ccccccc} \mathbf{I}\,\mathbf{0}\,\mathbf{0}\,\mathbf{0} & \mathbf{0}\,\mathbf{0}\,\mathbf{0}\,\mathbf{0} \\ \mathbf{0}\,\mathbf{I}\,\mathbf{0}\,\mathbf{0} & \mathbf{0}\,\mathbf{0}\,\mathbf{0}\,\mathbf{0} \\ \mathbf{0}\,\mathbf{0}\,\mathbf{I}\,\mathbf{0} & \mathbf{0}\,\mathbf{0}\,\mathbf{0}\,\mathbf{0} \end{array}\right] \tag{B63}$$

Matrices $\hat{\mathbf{N}}^{J}$ and $\mathbf{T}^{J}$ on the discontinuity:

$$\hat{\mathbf{N}}^{J} = \left[-\hat{N}_{(3)}\mathbf{I} \middle| -\hat{N}_{(1)}\mathbf{I} \middle| \hat{N}_{(3)}\mathbf{I} \middle| \hat{N}_{(1)}\mathbf{I} \right] \tag{B64}$$

$$\mathbf{T}^{J} = \left[\begin{array}{ccccccc} \mathbf{0}\,\mathbf{0}\,\mathbf{0}\,\mathbf{0} & \mathbf{0}\,\mathbf{0}\,\mathbf{I}\,\mathbf{0} \\ \mathbf{0}\,\mathbf{0}\,\mathbf{0}\,\mathbf{0} & \mathbf{I}\,\mathbf{0}\,\mathbf{0}\,\mathbf{0} \\ \mathbf{0}\,\mathbf{0}\,\mathbf{I}\,\mathbf{0} & \mathbf{0}\,\mathbf{0}\,\mathbf{0}\,\mathbf{0} \\ \mathbf{I}\,\mathbf{0}\,\mathbf{0}\,\mathbf{0} & \mathbf{0}\,\mathbf{0}\,\mathbf{0}\,\mathbf{0} \end{array}\right] \tag{B65}$$

B.4 Quadrangular element with special configuration for a discontinuity coinciding with only one node (Fig.B1 d)

Matrices $\hat{\mathbf{N}}^{-}$ and $\mathbf{T}^{-}$ for the quadrangular negative subdomain:

$$\hat{\mathbf{N}}^{-} = \left[\hat{N}^{-}_{(1)}\mathbf{I} \middle| \hat{N}^{-}_{(2)}\mathbf{I} \middle| \hat{N}^{-}_{(3)}\mathbf{I} \middle| \hat{N}^{-}_{(4)}\mathbf{I} \right] \tag{B66}$$

$$\mathbf{T}^{-} = \left[\begin{array}{ccccccc} \mathbf{I}\,\mathbf{0}\,\mathbf{0}\,\mathbf{0} & \mathbf{0}\,\mathbf{0}\,\mathbf{0}\,\mathbf{0} \\ \mathbf{0}\,\mathbf{0}\,\mathbf{0}\,\mathbf{0} & \mathbf{0}\,\mathbf{I}\,\mathbf{0}\,\mathbf{0} \\ \mathbf{0}\,\mathbf{0}\,\mathbf{I}\,\mathbf{0} & \mathbf{0}\,\mathbf{0}\,\mathbf{0}\,\mathbf{0} \\ \mathbf{0}\,\mathbf{0}\,\mathbf{0}\,\mathbf{I} & \mathbf{0}\,\mathbf{0}\,\mathbf{0}\,\mathbf{0} \end{array}\right] \tag{B67}$$

B.5 Quadrangular element with special configuration for a discontinuity coinciding with an edge (Fig.B1 e)

Matrices $\hat{\mathbf{N}}^-$ and $\mathbf{T}^-$ for the quadrangular negative subdomain:

$$\hat{\mathbf{N}}^- = \left[\hat{N}^-_{(1)}\mathbf{I} \middle| \hat{N}^-_{(2)}\mathbf{I} \middle| \hat{N}^-_{(3)}\mathbf{I} \middle| \hat{N}^-_{(4)}\mathbf{I} \right] \tag{B68}$$

$$\mathbf{T}^- = \left[\begin{array}{cccc|cccc} \mathbf{I} & \mathbf{0} & \mathbf{0} & \mathbf{0} & \mathbf{0} & \mathbf{0} & \mathbf{0} & \mathbf{0} \\ \mathbf{0} & \mathbf{0} & \mathbf{0} & \mathbf{0} & \mathbf{0} & \mathbf{I} & \mathbf{0} & \mathbf{0} \\ \mathbf{0} & \mathbf{0} & \mathbf{0} & \mathbf{0} & \mathbf{0} & \mathbf{0} & \mathbf{I} & \mathbf{0} \\ \mathbf{0} & \mathbf{0} & \mathbf{0} & \mathbf{I} & \mathbf{0} & \mathbf{0} & \mathbf{0} & \mathbf{0} \end{array}\right] \tag{B69}$$

Matrices $\hat{\mathbf{N}}^J$ and $\mathbf{T}^J$ on the discontinuity:

$$\hat{\mathbf{N}}^J = \left[-\hat{N}_{(3)}\mathbf{I} \middle| -\hat{N}_{(2)}\mathbf{I} \middle| \hat{N}_{(3)}\mathbf{I} \middle| \hat{N}_{(2)}\mathbf{I} \right] \tag{B70}$$

$$\mathbf{T}^J = \left[\begin{array}{cccc|cccc} \mathbf{0} & \mathbf{0} & \mathbf{0} & \mathbf{0} & \mathbf{0} & \mathbf{0} & \mathbf{I} & \mathbf{0} \\ \mathbf{0} & \mathbf{0} & \mathbf{0} & \mathbf{0} & \mathbf{0} & \mathbf{I} & \mathbf{0} & \mathbf{0} \\ \mathbf{0} & \mathbf{0} & \mathbf{I} & \mathbf{0} & \mathbf{0} & \mathbf{0} & \mathbf{0} & \mathbf{0} \\ \mathbf{0} & \mathbf{I} & \mathbf{0} & \mathbf{0} & \mathbf{0} & \mathbf{0} & \mathbf{0} & \mathbf{0} \end{array}\right] \tag{B71}$$

C INTERPOLATION MATRIX $\bar{\mathbf{N}}$ FOR TRIANGULAR ELEMENTS, AND SPECIAL CONFIGURATIONS

The geometry of the general case and special configurations of a triangular element crossed by a discontinuity and represented in Fig.C2

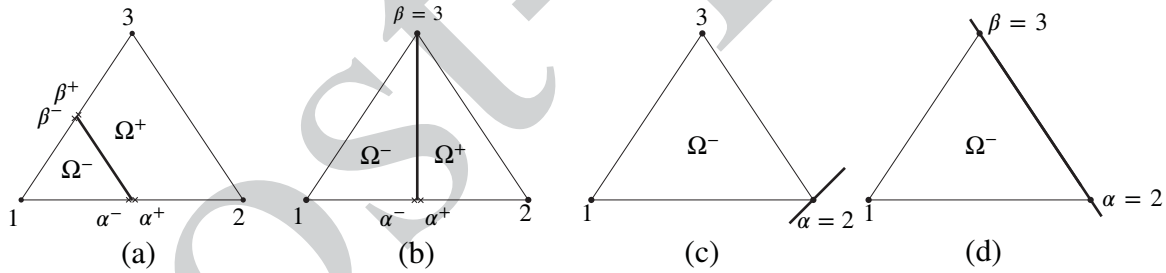

FIGURE C2 (a) General case of a triangular element crossed by the discontinuity. (b) Triangular element with special configuration for a discontinuity coinciding with one node and crossing an edge. (c) Triangular element with special configuration for a discontinuity coinciding with only one node. (d) Triangular element with special configuration for a discontinuity coinciding with an edge.

C.1 General matrices for triangular elements (Fig.C2 a)

Matrices $\hat{\mathbf{N}}^-$ and $\mathbf{T}^-$ for the triangular negative subdomain:

$$\hat{\mathbf{N}}^- = \left[\hat{N}^-_{(1)}\mathbf{I} \middle| \hat{N}^-_{(\alpha)}\mathbf{I} \middle| \hat{N}^-_{(\beta)}\mathbf{I} \right] \tag{C72}$$

$$\mathbf{T}^- = \left[\begin{array}{ccc|ccc} \mathbf{I} & \mathbf{0} & \mathbf{0} & \mathbf{0} & \mathbf{0} & \mathbf{0} \\ N_{(1)}(\alpha)\mathbf{I} & \mathbf{0} & \mathbf{0} & \mathbf{0} & N_{(2)}(\alpha)\mathbf{I} & \mathbf{0} \\ N_{(1)}(\beta)\mathbf{I} & \mathbf{0} & \mathbf{0} & \mathbf{0} & \mathbf{0} & N_{(3)}(\beta)\mathbf{I} \end{array}\right] \tag{C73}$$

Matrices $\hat{\mathbf{N}}^{+}$ and $\mathbf{T}^{+}$ for the triangular positive subdomain:

$$\hat{\mathbf{N}}^{+} = \left[\hat{N}^{+}_{(\alpha)}\mathbf{I} \middle| \hat{N}^{+}_{(2)}\mathbf{I} \middle| \hat{N}^{+}_{(3)}\mathbf{I} \middle| \hat{N}^{+}_{(\beta)}\mathbf{I} \right] \tag{C74}$$

$$\mathbf{T}^{+} = \left[\begin{array}{cccc|ccc} \mathbf{0} & N_{(2)}(\alpha)\mathbf{I} & \mathbf{0} & & N_{(1)}(\alpha)\mathbf{I} & \mathbf{0} & \mathbf{0} \\ \mathbf{0} & \mathbf{I} & \mathbf{0} & & \mathbf{0} & \mathbf{0} & \mathbf{0} \\ \mathbf{0} & \mathbf{0} & \mathbf{I} & & \mathbf{0} & \mathbf{0} & \mathbf{0} \\ \mathbf{0} & \mathbf{0} & N_{(3)}(\beta)\mathbf{I} & & N_{(1)}(\beta)\mathbf{I} & \mathbf{0} & \mathbf{0} \end{array}\right] \tag{C75}$$

Matrices $\hat{\mathbf{N}}^{J}$ and $\mathbf{T}^{J}$ on the discontinuity:

$$\hat{\mathbf{N}}^{J} = \left[-\hat{N}_{(\beta)}\mathbf{I} \middle| -\hat{N}_{(\alpha)}\mathbf{I} \middle| \hat{N}_{(\beta)}\mathbf{I} \middle| \hat{N}_{(\alpha)}\mathbf{I} \right] \tag{C76}$$

$$\mathbf{T}^{J} = \left[\begin{array}{ccc|ccc} \mathbf{N_{(1)}}(\boldsymbol{\beta})\mathbf{I} & \mathbf{0} & \mathbf{0} & \mathbf{0} & \mathbf{0} & N_{(3)}(\beta)\mathbf{I} \\ N_{(1)}(\alpha)\mathbf{I} & \mathbf{0} & \mathbf{0} & \mathbf{0} & N_{(2)}(\alpha)\mathbf{I} & \mathbf{0} \\ \mathbf{0} & \mathbf{0} & N_{(3)}(\beta)\mathbf{I} & N_{(1)}(\beta)\mathbf{I} & \mathbf{0} & \mathbf{0} \\ \mathbf{0} & N_{(2)}(\alpha)\mathbf{I} & \mathbf{0} & N_{(1)}(\alpha)\mathbf{I} & \mathbf{0} & \mathbf{0} \end{array}\right] \tag{C77}$$

C.2 Triangular element with special configuration for a discontinuity coinciding with one node and crossing an edge (Fig.C2 b)

Matrices $\hat{\mathbf{N}}^{-}$ and $\mathbf{T}^{-}$ for the triangular negative subdomain:

$$\hat{\mathbf{N}}^{-} = \left[\hat{N}^{-}_{(1)}\mathbf{I} \middle| \hat{N}^{-}_{(\alpha)}\mathbf{I} \middle| \hat{N}^{-}_{(3)}\mathbf{I} \right] \tag{C78}$$

$$\mathbf{T}^{-} = \left[\begin{array}{ccc|ccc} \mathbf{I} & \mathbf{0} & \mathbf{0} & \mathbf{0} & \mathbf{0} & \mathbf{0} \\ N_{(1)}(\alpha)\mathbf{I} & \mathbf{0} & \mathbf{0} & \mathbf{0} & N_{(2)}(\alpha)\mathbf{I} & \mathbf{0} \\ \mathbf{0} & \mathbf{0} & \mathbf{0} & \mathbf{0} & \mathbf{0} & \mathbf{I} \end{array}\right] \tag{C79}$$

Matrices $\hat{\mathbf{N}}^{+}$ and $\mathbf{T}^{+}$ for the triangular positive subdomain:

$$\hat{\mathbf{N}}^{+} = \left[\hat{N}^{+}_{(\alpha)}\mathbf{I} \middle| \hat{N}^{+}_{(2)}\mathbf{I} \middle| \hat{N}^{+}_{(3)}\mathbf{I} \right] \tag{C80}$$

$$\mathbf{T}^{+} = \left[\begin{array}{ccc|ccc} \mathbf{0} & N_{(2)}(\alpha)\mathbf{I} & \mathbf{0} & N_{(1)}(\alpha)\mathbf{I} & \mathbf{0} & \mathbf{0} \\ \mathbf{0} & \mathbf{I} & \mathbf{0} & \mathbf{0} & \mathbf{0} & \mathbf{0} \\ \mathbf{0} & \mathbf{0} & \mathbf{I} & \mathbf{0} & \mathbf{0} & \mathbf{0} \end{array}\right] \tag{C81}$$

Matrices $\hat{\mathbf{N}}^{J}$ and $\mathbf{T}^{J}$ on the discontinuity:

$$\hat{\mathbf{N}}^{J} = \left[-\hat{N}_{(\beta)}\mathbf{I} \middle| -\hat{N}_{(\alpha)}\mathbf{I} \middle| \hat{N}_{(\beta)}\mathbf{I} \middle| \hat{N}_{(\alpha)}\mathbf{I} \right] \tag{C82}$$

$$\mathbf{T}^{J} = \left[\begin{array}{ccc|ccc} \mathbf{0} & \mathbf{0} & \mathbf{0} & \mathbf{0} & \mathbf{0} & \mathbf{I} \\ N_{(1)}(\alpha)\mathbf{I} & \mathbf{0} & \mathbf{0} & \mathbf{0} & N_{(2)}(\alpha)\mathbf{I} & \mathbf{0} \\ \mathbf{0} & \mathbf{0} & \mathbf{I} & \mathbf{0} & \mathbf{0} & \mathbf{0} \\ \mathbf{0} & N_{(2)}(\alpha)\mathbf{I} & \mathbf{0} & N_{(1)}(\alpha)\mathbf{I} & \mathbf{0} & \mathbf{0} \end{array}\right] \tag{C83}$$

C.3 Triangular element with special configuration for a discontinuity coinciding with only one node (Fig.C2 c)

Matrices $\hat{\mathbf{N}}^{-}$ and $\mathbf{T}^{-}$ for the triangular negative subdomain:

$$\hat{\mathbf{N}}^{-} = \left[\hat{N}^{-}_{(1)}\mathbf{I} \middle| \hat{N}^{-}_{(2)}\mathbf{I} \middle| \hat{N}^{-}_{(3)}\mathbf{I} \right] \tag{C84}$$

$$\mathbf{T}^{-} = \left[\begin{array}{ccc|ccc} \mathbf{I} & \mathbf{0} & \mathbf{0} & \mathbf{0} & \mathbf{0} & \mathbf{0} \\ \mathbf{0} & \mathbf{0} & \mathbf{0} & \mathbf{0} & \mathbf{I} & \mathbf{0} \\ \mathbf{0} & \mathbf{0} & \mathbf{I} & \mathbf{0} & \mathbf{0} & \mathbf{0} \end{array}\right] \tag{C85}$$

C.4 Triangular element with special configuration for a discontinuity coinciding with an edge (Fig.C2 d)

Matrices $\hat{\mathbf{N}}^{-}$ and $\mathbf{T}^{-}$ for the triangular negative subdomain:

$$\hat{\mathbf{N}}^{-} = \left[\begin{array}{c|c|c} \hat{N}^{-}_{(1)}\mathbf{I} & \hat{N}^{-}_{(2)}\mathbf{I} & \hat{N}^{-}_{(3)}\mathbf{I} \end{array}\right] \tag{C86}$$

$$\mathbf{T}^{-} = \left[\begin{array}{ccc|ccc} \mathbf{I} & \mathbf{0} & \mathbf{0} & \mathbf{0} & \mathbf{0} & \mathbf{0} \\ \mathbf{0} & \mathbf{0} & \mathbf{0} & \mathbf{0} & \mathbf{I} & \mathbf{0} \\ \mathbf{0} & \mathbf{0} & \mathbf{0} & \mathbf{0} & \mathbf{0} & \mathbf{I} \end{array}\right] \tag{C87}$$

Matrices $\hat{\mathbf{N}}^{J}$ and $\mathbf{T}^{J}$ on the discontinuity:

$$\hat{\mathbf{N}}^{J} = \left[\begin{array}{c|c|c|c} -\hat{N}_{(3)}\mathbf{I} & -\hat{N}_{(2)}\mathbf{I} & \hat{N}_{(3)}\mathbf{I} & \hat{N}_{(2)}\mathbf{I} \end{array}\right] \tag{C88}$$

$$\mathbf{T}^{J} = \left[\begin{array}{cccc|cccc} \mathbf{0} & \mathbf{0} & \mathbf{0} & \mathbf{0} & \mathbf{0} & \mathbf{0} & \mathbf{I} & \mathbf{0} \\ \mathbf{0} & \mathbf{0} & \mathbf{0} & \mathbf{0} & \mathbf{0} & \mathbf{I} & \mathbf{0} & \mathbf{0} \\ \mathbf{0} & \mathbf{0} & \mathbf{I} & \mathbf{0} & \mathbf{0} & \mathbf{0} & \mathbf{0} & \mathbf{0} \\ \mathbf{0} & \mathbf{I} & \mathbf{0} & \mathbf{0} & \mathbf{0} & \mathbf{0} & \mathbf{0} & \mathbf{0} \end{array}\right] \tag{C89}$$

D FORMULATION BASED ON NATURAL SHAPE FUNCTIONS, SPURIOUS OSCILLATIONS AND INTERPRETATION

The "natural" interpolation scheme, generally assumed in existing XFEM formulations, represented in Figure D3 , is based on the following assumptions:

1. The discontinuity subdivides element in two subdomains, crossing element edges at intersection points α and β, with local coordinates $\boldsymbol{r}_{\alpha}$, $\boldsymbol{r}_{\beta}$ and classical Gauss points are defined within each subdomain (Fig. D3 a)
2. classical interpolation functions of the original element (Fig. D3 c) are used to interpolate the main variable in terms of the original nodal variables (regular $\boldsymbol{u}_k$ and additional $\boldsymbol{\delta}_k$). For points in the negative and positive subdomains this gives:

$$\boldsymbol{u}^{-}(\boldsymbol{r}) = N_{(1)}(\boldsymbol{r})\,\boldsymbol{u}_{(1)} + N_{(2)}(\boldsymbol{r})\,\boldsymbol{\delta}_{(2)} + N_{(3)}(\boldsymbol{r})\,\boldsymbol{\delta}_{(3)} + N_{(4)}(\boldsymbol{r})\,\boldsymbol{u}_{(4)} \tag{D90}$$

$$\boldsymbol{u}^{+}(\boldsymbol{r}) = N_{(1)}(\boldsymbol{r})\,\boldsymbol{\delta}_{(1)} + N_{(2)}(\boldsymbol{r})\,\boldsymbol{u}_{(2)} + N_{(3)}(\boldsymbol{r})\,\boldsymbol{u}_{(3)} + N_{(4)}(\boldsymbol{r})\,\boldsymbol{\delta}_{(4)} \tag{D91}$$

In order to better interpret the consequences of these assumptions and compare to the new approach proposed with sub-interpolation, it is convenient to replace the additional variables at the nodes $\boldsymbol{\delta}_k$ ($k = 1, 4$) by the physical displacements at the negative and positive sides of the intersection points $\boldsymbol{u}^{-}_{(\alpha)}$,$\boldsymbol{u}^{+}_{(\alpha)}$,$\boldsymbol{u}^{-}_{(\beta)}$,$\boldsymbol{u}^{+}_{(\beta)}$. This is achieved by considering first the linear interpolation along element edge 1-2 (where $N_{(3)} = N_{(4)} = 0$):

$$\boldsymbol{u}^{-}_{(\alpha)} = \boldsymbol{u}^{-}\left(\boldsymbol{r}_{(\alpha)}\right) = N_{(1)}\left(\boldsymbol{r}_{(\alpha)}\right)\boldsymbol{u}_{(1)} + N_{(2)}\left(\boldsymbol{r}_{(\alpha)}\right)\boldsymbol{\delta}_{(2)} \tag{D92}$$

$$\boldsymbol{u}^{+}_{(\alpha)} = \boldsymbol{u}^{+}\left(\boldsymbol{r}_{(\alpha)}\right) = N_{(1)}\left(\boldsymbol{r}_{(\alpha)}\right)\boldsymbol{\delta}_{(1)} + N_{(2)}\left(\boldsymbol{r}_{(\alpha)}\right)\boldsymbol{u}_{(2)} \tag{D93}$$

from which one obtains:

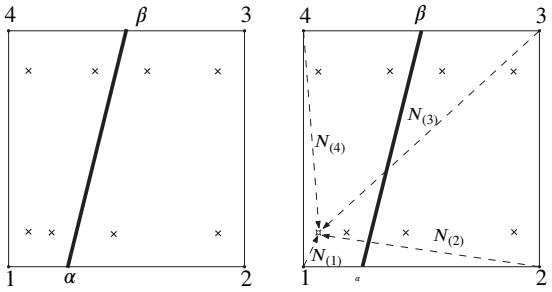

FIGURE D3 Natural interpolation: (a) Intersection points α, β and subdomain Gauss points location. (b) Standard interpolation functions $N_{(i)}$ of the global element are used already to interpolate nodal variables to the subdomain Gauss points.

$$\boldsymbol{\delta}_{(2)} = \frac{1}{N_{(2)}\left(\boldsymbol{r}_{(\alpha)}\right)} \bar{\boldsymbol{u}}_{(\alpha)} - \frac{N_{(1)}\left(\boldsymbol{r}_{(\alpha)}\right)}{N_{(2)}\left(\boldsymbol{r}_{(\alpha)}\right)} \boldsymbol{u}_{(1)} \tag{D94}$$

$$\boldsymbol{\delta}_{(1)} = \frac{1}{N_{(1)}\left(\boldsymbol{r}_{(\alpha)}\right)} \bar{\boldsymbol{u}}_{(\alpha)} - \frac{N_{(2)}\left(\boldsymbol{r}_{(\alpha)}\right)}{N_{(1)}\left(\boldsymbol{r}_{(\alpha)}\right)} \boldsymbol{u}_{(2)} \tag{D95}$$

By doing similarly along edge 3-4 one obtains:

$$\boldsymbol{\delta}_{(4)} = \frac{1}{N_{(4)}\left(\boldsymbol{r}_{(\beta)}\right)} \bar{\boldsymbol{u}}_{(\beta)} - \frac{N_{(3)}\left(\boldsymbol{r}_{(\beta)}\right)}{N_{(4)}\left(\boldsymbol{r}_{(\beta)}\right)} \boldsymbol{u}_{(3)} \tag{D96}$$

$$\boldsymbol{\delta}_{(3)} = \frac{1}{N_{(3)}\left(\boldsymbol{r}_{(\beta)}\right)} \bar{\boldsymbol{u}}_{(\beta)} - \frac{N_{(4)}\left(\boldsymbol{r}_{(\beta)}\right)}{N_{(3)}\left(\boldsymbol{r}_{(\beta)}\right)} \boldsymbol{u}_{(4)} \tag{D97}$$

Replacing now (D94-D95) and (D96-D97) into equation (D92) leads to the new interpolation expression for the negative subdomain

$$\bar{\boldsymbol{u}}(\boldsymbol{r}) = \hat{N}^{-}_{(1)}(\boldsymbol{r})\,\boldsymbol{u}_{(1)} + \hat{N}^{-}_{(\alpha)}(\boldsymbol{r})\,\bar{\boldsymbol{u}}_{(\alpha)} + \hat{N}^{-}_{(\beta)}(\boldsymbol{r})\,\bar{\boldsymbol{u}}_{(\beta)} + \hat{N}^{-}_{(4)}(\boldsymbol{r})\,\boldsymbol{u}_{(4)} \tag{D98}$$

where $\hat{N}^{-}_{(1)}$, $\hat{N}^{-}_{(\alpha)}$, $\hat{N}^{-}_{(\beta)}$ and $\hat{N}^{-}_{(4)}$ are the subdomain local interpolation functions in terms of the displacement values at the corners of that subdomain, with expressions:

$$\hat{N}^{-}_{(1)}(\boldsymbol{r}) = N_{(1)}(\boldsymbol{r}) - \frac{N_{(1)}\left(\boldsymbol{r}_{(\alpha)}\right)}{N_{(2)}\left(\boldsymbol{r}_{(\alpha)}\right)} N_{(2)}(\boldsymbol{r}) \tag{D99}$$

$$\hat{N}^{-}_{(\alpha)}(\boldsymbol{r}) = \frac{1}{N_{(2)}\left(\boldsymbol{r}_{(\alpha)}\right)} N_{(2)}(\boldsymbol{r}) \tag{D100}$$

$$\hat{N}^{-}_{(\beta)}(\boldsymbol{r}) = \frac{1}{N_{(3)}\left(\boldsymbol{r}_{(\beta)}\right)} N_{(3)}(\boldsymbol{r}) \tag{D101}$$

$$\hat{N}^{-}_{(4)}(\boldsymbol{r}) = N_{(4)}(\boldsymbol{r}) - \frac{N_{(4)}\left(\boldsymbol{r}_{(\alpha)}\right)}{N_{(3)}\left(\boldsymbol{r}_{(\alpha)}\right)} N_{(3)}(\boldsymbol{r}) \tag{D102}$$

(D103)

Consider now the edge $\alpha - \beta$ of this negative sub-element, which coincides with the discontinuity line. A basic finite element requirement for inter-element continuity (conformity) is that the interpolation on any element edge or face should depend only on the nodal variables on the same element edge or face (and not on the nodal variables of any other node of the element). In this case, this means that the displacement value along that edge should not depend on $\boldsymbol{u}_{(1)}$ or $\boldsymbol{u}_{(4)}$, and the only way for that to happen is if $\hat{N}^{-}_{(1)}$ and $\hat{N}^{-}_{(4)}$ both vanish along that edge, that is, if

$$\hat{N}^{-}_{(1)}(\boldsymbol{r}) = N_{(1)}(\boldsymbol{r}) - \frac{N_{(1)}(\boldsymbol{r}_{(\alpha)})}{N_{(2)}(\boldsymbol{r}_{(\alpha)})} N_{(2)}(\boldsymbol{r}) = 0 \tag{D104}$$

$$\hat{N}^{-}_{(4)}(\boldsymbol{r}) = N_{(4)}(\boldsymbol{r}) - \frac{N_{(4)}(\boldsymbol{r}_{(\alpha)})}{N_{(3)}(\boldsymbol{r}_{(\alpha)})} N_{(3)}(\boldsymbol{r}) = 0 \tag{D105}$$

(D106)

In the Q4 linear element considered, this only can happen along lines parallel to edges $1-4$ and $2-3$ (parallel in the sense of local coordinates), and therefore this means that the local interpolation functions implied by natural interpolation cannot satisfy the conformity requirement along the discontinuity line in the general case that the discontinuity runs skew to the FE mesh. Similarly, for the positive subdomain the interpolation expression reads

$$\boldsymbol{u}^{+}(\boldsymbol{r}) = \hat{N}^{+}_{(\alpha)}(\boldsymbol{r})\,\boldsymbol{u}^{+}_{(\alpha)} + \hat{N}^{+}_{(2)}(\boldsymbol{r})\,\boldsymbol{u}_{(2)} + \hat{N}^{+}_{(3)}(\boldsymbol{r})\,\boldsymbol{u}_{(3)} + \hat{N}^{+}_{(\beta)}(\boldsymbol{r})\,\boldsymbol{u}^{+}_{(\beta)} \tag{D107}$$

with the local subdomain interpolation functions

$$\hat{N}^{+}_{(\alpha)}(\boldsymbol{r}) = \frac{1}{N_{(1)}(\boldsymbol{r}_{(\alpha)})} N_{(1)}(\boldsymbol{r}) \tag{D108}$$

$$\hat{N}^{+}_{(2)}(\boldsymbol{r}) = N_{(2)}(\boldsymbol{r}) - \frac{N_{(2)}(\boldsymbol{r}_{(\alpha)})}{N_{(1)}(\boldsymbol{r}_{(\alpha)})} N_{(1)}(\boldsymbol{r}) \tag{D109}$$

$$\hat{N}^{+}_{(3)}(\boldsymbol{r}) = N_{(3)}(\boldsymbol{r}) - \frac{N_{(3)}(\boldsymbol{r}_{(\alpha)})}{N_{(4)}(\boldsymbol{r}_{(\alpha)})} N_{(4)}(\boldsymbol{r}) \tag{D110}$$

$$\hat{N}^{+}_{(\beta)}(\boldsymbol{r}) = \frac{1}{N_{(4)}(\boldsymbol{r}_{(\beta)})} N_{(4)}(\boldsymbol{r}) \tag{D111}$$

(D112)

The conformity condition would require in this case that $\hat{N}^{+}_{(2)}(\boldsymbol{r})$ and $\hat{N}^{+}_{(3)}(\boldsymbol{r})$ vanish along the discontinuity line, which can only happen if that line is parallel (in the sense of local coordinates) to the element edges, and therefore the conditions *cannot* be satisfied for skew discontinuities. Figure D4 depicts the local subdomain shape functions in elements where the discontinuity is not parallel to the element faces. Shape functions of original nodes $\hat{N}^{-}_{(1)}$, $\hat{N}^{+}_{(2)}$, $\hat{N}^{+}_{(3)}$ and $\hat{N}^{-}_{(4)}$ do not vanish along the discontinuity line as one would expect. Shape functions of intersection points $\hat{N}^{-}_{(\alpha)}$, $\hat{N}^{-}_{(\beta)}$, $\hat{N}^{+}_{(\alpha)}$ and $\hat{N}^{+}_{(\beta)}$ are non-linear along the discontinuity line and, as shown in the last two diagrams, do not coincide one-to-one along that line even in the case that the two nodes of each pair would take the same values.

Therefore, it is not surprising that when the discontinuity is skew to the mesh lines this scheme leads to spurious oscillations (although these oscillations may be reduced by mesh refinement), as seen in Figures D6 and D7 . Note that all these problems disappear in the new scheme proposed with sub-interpolation, since displacement fields along the discontinuity line become linear and conformity is guaranteed.

The above arguments are illustrated with the following example of application consisting of a short rectangular beam of 4×1m subject to axial tension, which is crossed by a skew XFEM elastic discontinuity (Fig. D5). The load is applied via horizontal displacement of value $u_x = 0.001$m, on the right end of the beam, while horizontal movement on the left end is prescribed to zero. In this example, small deformations, plane strain and isotropic elastic material are assumed, with Young modulus $E = 1000$MPa, Poisson's ratio $\nu = 0$, and XFEM discontinuity stiffness has been assumed very high $K_N = K_T = 10^8$MPa/s.

Note that with the high values assumed for K_N, K_T, the case analyzed should correspond to uniform uniaxial tension, and stress on the discontinuity should be constant and equal to the normal and shear stress projections on the plane oriented with the discontinuity, of that uniaxial state.

The stress values obtained solving that problem with natural interpolation and sub-interpolation are depicted in Fig. D6 (continuum) and D7 (discontinuity). In order to discriminate the possible effect of the integration rule along the discontinuity segments contained within each element, the calculations have been repeated using three different integration rules: trapezoidal

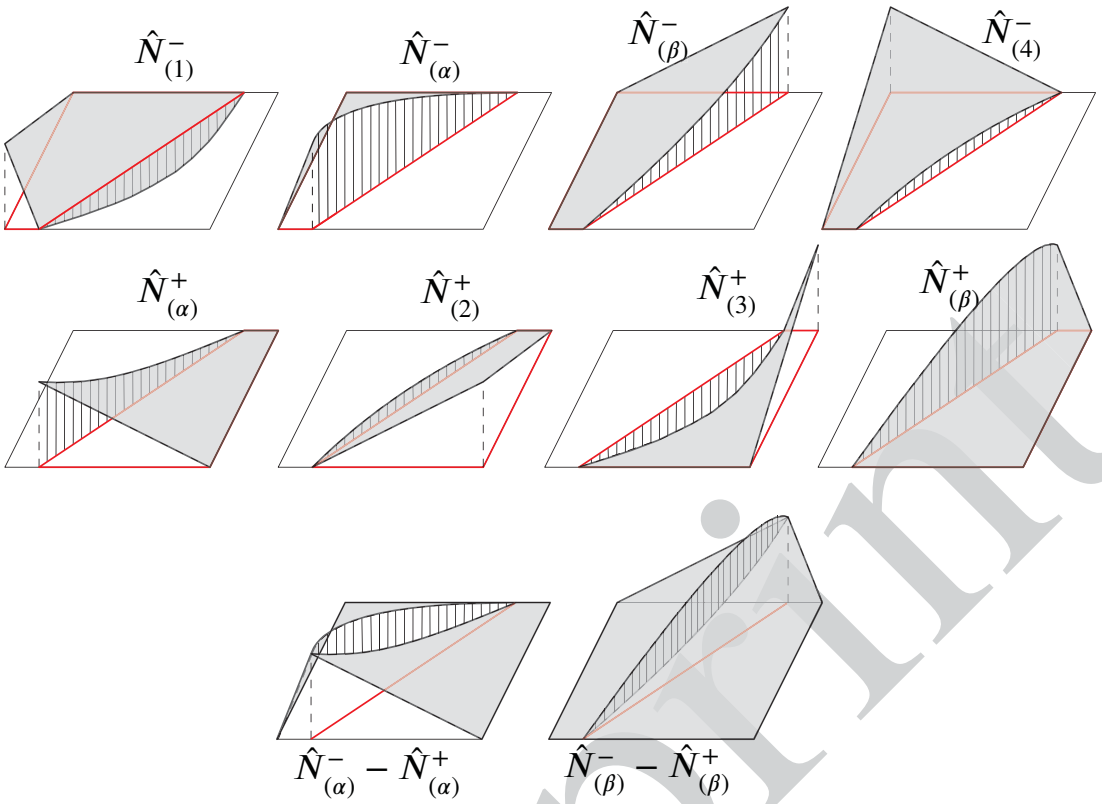

FIGURE D4 Subdomain shape functions used in the natural interpolation.

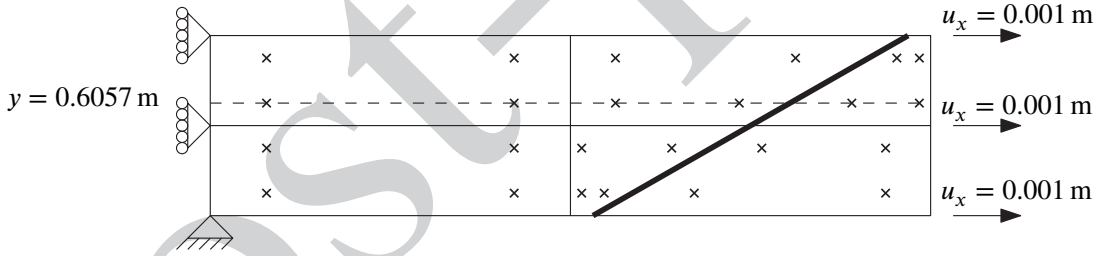

FIGURE D5 Short rectangular beam of 4 × 1m discretized into four quadrangular elements and crossed by an inclined discontinuity (bold line). Crosses represent Gauss points of the resulting elements and subdomains.

rule, Gauss 2-points rule and Simpson's rule. Using natural interpolation, stresses in the continuum (Fig. D6) turn out not constant, varying from $\sigma_x = 0.2203$MPa to $\sigma_x = 0.2618$MPa, while the correct result should be $\sigma_x = 0.2500$MPa, as it is obtained correctly using double interpolation (Fig. D6 a). Also σ_{yy} and τ_{xy} should be identically zero in this uniaxial case, and this is correct with double interpolation while natural interpolation leads to spurious non-zero values. Note that the stress values in the continuum are the same for the three integration rules along the discontinuity.

Stress tractions along the discontinuity, represented in Fig. D7 , reflect the same situation. Double interpolation leads to the correct constant values of normal and tangential stress tractions $\sigma_j = 0.0589$m and $\tau_j = 0.1061$MPa, while natural solution oscillates significantly for any of the three integration rules used.

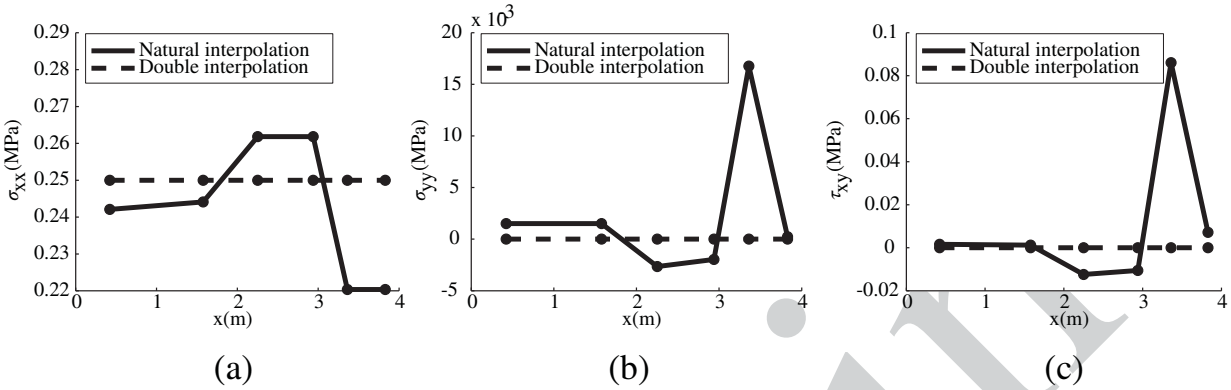

FIGURE D6 Stress component values along a horizontal line containing the Gauss points at $y = 0.6057$m. The solid line corresponds to the traditional XFEM formulation with natural interpolation (same results for all integration rules along the discontinuity), and the dashed line for the formulation described with double interpolation. (a) σ_{xx}, (b) σ_{yy} and (c) σ_{xy}.

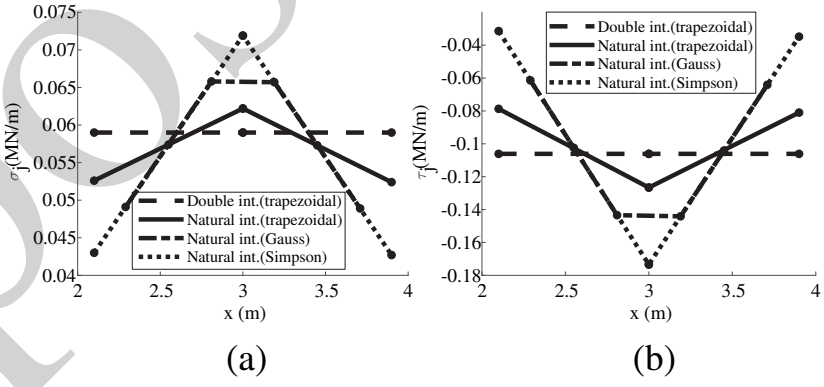

FIGURE D7 Stress field along the discontinuity line obtained using threee different integration rules along the dicontinuity section corresponding to each element: (a) Normal component, σ_j. (b) Tangential component, τ_j.